PHYSICS - BASED THERMO - MECHANICAL FATIGUE MODEL FOR LIFE PREDICTION OF HIGH TEMPERATURE ALLOYS

by

Abhilash Anilrao Gulhane

A Thesis

Submitted to the Faculty of Purdue University

In Partial Fulfillment of the Requirements for the degree of

Master of Science in Mechanical Engineering

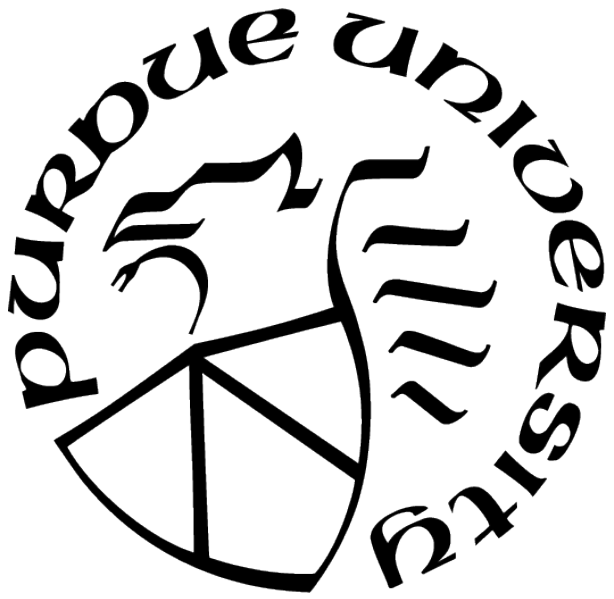

Department of Mechanical and Energy Engineering

Indianapolis, Indiana

May 2021

THE PURDUE UNIVERSITY GRADUATE SCHOOL
STATEMENT OF COMMITTEE APPROVAL

Dr. Jing Zhang, Chair

Department of Mechanical and Energy Engineering, IUPUI

Dr. Sohel Anwar

Department of Mechanical and Energy Engineering, IUPUI

Dr. Likun Zhu

Department of Mechanical and Energy Engineering, IUPUI

Approved by:

Dr. Jie Chen

Dedicated to

My parents for their enormous motivation

My uncle for his belief in me,

And to the light of my life for her constant support

ACKNOWLEDGMENTS

I would like to thank Dr. Jing Zhang for his support during the research and giving me opportunity to present at various conferences during my master's journey. I would not have achieved this without his enormous support and guidance throughout.

I would like to thank Dr. Anwar and Dr. Zhu for serving as part of my advisory committee.

I would also like to thank my lab mates Harshal, Jian, Anvesh and Tejesh for their help.

TABLE OF CONTENTS

LIST OF TABLES

LIST OF FIGURES

ABBREVIATIONS

FEA	Finite Element Analysis
LCF	Low Cycle Fatigue
LCFC	Low Cycle Fatigue Creep
TMF	Thermal-Mechanical Fatigue
ODE	Ordinary Differential Equation
DCI	Ductile Cast Iron

ABSTRACT

High temperature alloys have been extensively used in many applications, such as furnace muffles, fuel nozzles, heat treating fixtures and fuel nozzles. Due to such conditions these materials should have resistance to cyclic loading, oxidation and high heat. Although there are numerous prior experimental and theoretical studies, there is insufficient understanding of application of the unified viscoplasticity theory to finite element software for fatigue life prediction.

Therefore, the goal of this research is to develop a procedure to implement unified viscoplasticity theory in finite element (FE) model to model the complex material deformation pertaining to thermomechanical load and implement an incremental damage lifetime rule to predict thermomechanical fatigue life of high temperature alloys.

The objectives of the thesis are:

1. Develop a simplified integrated approach to model the fatigue creep deformation under the framework of 'unified viscoplasticity theory'

2. Implement a physics - based crack growth damage model into the framework

3. Predict the deformation using the unified viscoplastic material model for ferritic cast iron (Fe-3.2C-4.0Si-0.6Mo) SiMo4.06

4. Predict the isothermal low cycle fatigue (LCF) and LCF-Creep life using the damage model

In this work, a unified viscoplastic material model is applied in a FE model with a combination of Chaboche non-linear kinematic hardening, Perzyna rate model and static recovery model to model rate dependent plasticity, stress relaxation, and creep-fatigue interaction. Also, an incremental damage rule has been successfully implemented in a FE model. The calibrated viscoplastic model is able to correlate deformations pertaining to isothermal LCF, LCF-Creep and thermal-mechanical fatigue (TMF) experimental deformations. The life predictions from the FE model have been fairly good at room temperature (20°C), 400°C and 550°C under Isothermal LCF (0.00001/s and 0.003/s) and LCF-Creep tests.

The material calibration techniques proposed for calibrating the model parameters resulted in a fairly good correlation of FE model derived hysteresis loops with experimental hysteresis, pertaining to Isothermal LCF (ranging from 0.00001/s to 0.003/s), Isothermal LCF-Creep tests (with hold time) and TMF responses. In summary, the method and models developed in this work are capable of simulating material deformation dependency on temperature, strain-rates, hold time, therefore, they are capable to modeling creep-stress relaxation and fatigue interaction in high-temperature alloy design.

1. INTRODUCTION

1.1 Literature Review

A variety of metallic components across the transportation, aviation, power, and electronics industry are operated at high temperature and experience complex thermal-mechanical loads. For instance, in thermal power plant segment in order to improve efficiency and comply with the emmission standards these power plants are operated at peak steam temperature of 760C and pressure as high as 350 bar. In the electronic industry, the increasing power density and usage in harsh environments experiences cyclic thermal-mechanical loads on the PCB's, solder joints and the electronic packaging. Whereas in the transportation industry, the internal combustion engine components undergo rapid cyclic thermal loads and vibrations [1].

In the design and reliability analysis of mechanical components, the performance of high temperature components is a primary concern, especially in determining their safe life. At high temperatures the material response become strain rate sensitive and other mechanisms like creep and oxidation influences the overall durability and life of the components and are often the primary damage mechanisms causing the failure.

In metals the predominant damage mechanisms are creep, fatigue and oxidation. It is known that the damage due to fatigue load is not instantaneous, but it is a result of a steady accumulation of damage and it depends upon the loading history. During the fatigue response, various complex damage mechanisms act, which depends on the thermal and mechanical loads and boundary conditions and also upon the material microstructure.

Therefore, for investigation of the failure mechanisms of components in response to thermomechanical loading, it is necessary to have advanced numerical material models that can simulate the complex material deformation and also can accurately predict the damage accumulation. In particular, first it is required to have a constitutive deformation model capable of simulating complex material behaviour, and secondly a damage accumulation model which can accurately predict fatigue life.

1.1.1 Review of Plasticity Models

The total strain can be partitioned into thermal strain and mechanical strain, where the mechanical strain is further partitioned into elastic and viscoplastic strains as described in Equation 1.1 and Equation 1.2. The constitutive modeling of the viscoplastic strain has traditionally followed a non-unified approach where the cyclic plastic strain and creep strain are partitioned as described in Equation 1.3.

$$\varepsilon_T = \varepsilon_m + \varepsilon_{th} \tag{1.1}$$

$$\varepsilon_m = \varepsilon_{\mathrm{e}} + \varepsilon_{vp} \tag{1.2}$$

$$\varepsilon_{vp} = \varepsilon_{pl} + \varepsilon_{cr} \tag{1.3}$$

Non-unified models, which consider the partition between plastic and creep strains, have been found to be incapable of predicting acceptably certain deformation features such as cyclic creep, also known as ratcheting, and creep-plasticity interaction [2], [3].

The constitutive models for creep have been done separately from cyclic viscoplasticity models, based upon various phases (primary, secondary, and tertiary) of creep responses. As a result, the creep equations which have been developed are exclusively for the creep responses where the rate process of creep, which is thermally activated, is modelled using the Arrhenius type of temperature dependant equation. These creep models are developed without considering the interactions of viscoplasticity and their constitutive framework is not applicable to cyclic response simulations [3]. Also, since the combined effect of plasticity and creep is measurable, as shown in experiments of Niitsu [4] the associative hardening effects of coupling plastic and creep strains, they cannot be treated separately. Thus, non-unified approaches are incapable of predicting certain deformations such cyclic creep and creep-plasticity interaction. Therefore, there is a need to implement constitutive deformation models which can represent inelastic deformation such as plasticity, creep, and stress relaxation as a single inelastic strain.[3]

1.1.2 Review of Damage Model

Various parametric damage models are available such as models-based on plastic strains like Coffin-Mansion, stress-based models like Basquin, Goodman, Walker, and energy-based models like Dasgupta. Parametric models are often based on strain partitioning and considers the damage accumulation due to various damage mechanisms explicitly by additive life fraction rule, as expressed in equation 1.4.

$$\frac{1}{N_{\mathrm{f}}} = \frac{1}{N_{\mathrm{fat}}} + \frac{1}{N_{\mathrm{cr}}} + \frac{1}{N_{\mathrm{ox}}} \tag{1.4}$$

There are also approaches such as the accelerated cyclic integration approach or the cycle jump method in which the solution variables are extrapolated by jumping over the intermediate cycles and mathematically expressed as the global long-term trend, as shown in Figure 1.1.

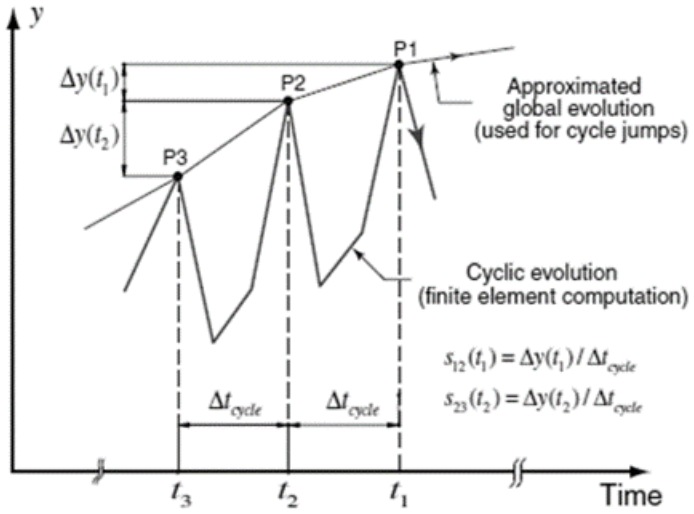

Figure 1.1. A schematic of a cycle jump method in FEA [5]

Above approaches, like the Parametric modelling are often based on strain partitioning and considers the damage accumulation due to various damage mechanisms explicitly by additive life fraction rule, as expressed in equation 1.4. Such models cannot reproduce the dependency of damage on cycle times (strain rate), temperature, stress and strain history appropriately [6]

Besides, these lifetime rules are not advantageous since they do not consider the complex loading path or the loading histories so that complex histories like creep-fatigue interaction and multiaxial loading can be evaluated. Such models use a purely phenomenological model for fatigue. Hence lifetime models are needed that refer to the physics-based damage mechanism, namely the growth of cracks, and that are able to reproduce the dependency of crack growth rates on cycle times, strain amplitudes, mean stress, and temperature [6]

1.2 Motivation

Given the above discussion, it is noted that although there are numerous prior experimental and theoretical studies, there is insufficient understanding of application of the unified viscoplasticity theory to finite element software for fatigue life prediction. To investigate the failure mechanisms of components in response to thermomechanical loading, it is necessary to have advanced numerical material models that can describe the complex material behaviour and can accurately predict the deformation and damage accumulation. In particularly, the following studies are needed:

1. A constitutive deformation model which can represent total inelastic strain, which is plastic strain and creep strain, as a combined inelastic strain

2. Damage models that can take into consideration the deformation history (in response to thermo-mechanical loads) and the physics (crack growth) to evaluate fatigue life

1.3 Goal and Objective

The goal of this research is to develop a procedure to implement unified viscoplasticity theory in finite element (FE) model to model the complex material deformation pertaining to thermomechanical load and implement an incremental damage lifetime rule to predict thermomechanical fatigue life of high temperature alloys. Also, in addition to this another objective is to model the high temperature, fatigue -creep deformation of Ferritic Ductile Cast

Iron (Fe-3.2C-4.0Si-0.6Mo) in response to isothermal LCF, LCF-Creep and non-isothermal TMF loading and to predict crack initiation life of SiMo4.06 using Finite Element Method.

This research is therefore focused on the following objectives:

1. To develop a simplified integrated approach to model the fatigue creep deformation under the framework of 'Unified Viscoplasticity theory'
2. Implement a physics - based crack growth damage model into the framework
3. Predict the deformation using the Unified Viscoplastic material model for ferritic cast iron
4. Predict the isothermal LCF and LCF-Creep life using the damage model

1.4 Structure of the Thesis

The structure of the thesis is such that, the formulation of the physics-based damage model is discussed in chapter 2, followed by the application of the damage model for fatigue life prediction is discussed in chapter 3, while chapter 4 is about FEA predictions and results

2. FORMULATION OF PHYSICS-BASED DAMAGE MODEL

Formulation of a damage model firstly requires modelling of deformation to accurately predict the deformation in response to thermomechanical loads, followed by damage modelling. Thus, in following sections formulation and plasticity modelling is discussed, followed by damage modelling.

2.1 Formulation of Unified Viscoplasticity Model

The formulation of the Viscoplastic model involves following steps and discussed below:

1. Flow rule
2. Kinematic hardening rules

2.1.1 Viscoplasticity Theory and Flow Rule

The unified viscoplasticity theory, accounts for all the aspects of creep, plasticity and stress relaxation are represented by a single inelastic quantity. In viscoplasticity theory, chaboche described the stress in excess of yield surface as overstress or viscous stress [7]. Chaboche also showed that the relationship between the viscous stress and the plastic strain rate norm is highly non-linear which formed the basis of flow rule as expressed in Equation 2.1. [8]

$$\dot{p} = \left\langle \frac{\sigma_v}{K} \right\rangle^n \tag{2.1}$$

Thus, the overstress forms the basic quantity to define viscoplastic potential [3], such that the inelastic or viscoplastic strain rate is obtained from equation 2.2 as,

$$\dot{\varepsilon}^{vp} = \frac{\partial \Omega}{\partial \sigma} = \frac{3}{2}\dot{p}\frac{s - \mathbf{a}}{J(\sigma - \alpha)} \tag{2.2}$$

Where J(sigma - a) is the von-misses invariant expressed as:

$$J(\sigma - \boldsymbol{\alpha}) = \left[\frac{3}{2}(\ \mathrm{s} - \mathbf{a}) : (\mathrm{s} - \mathbf{a})\right]^{\frac{1}{2}} \tag{2.3}$$

And the von-misses criteria used is:

$$f(\boldsymbol{\sigma} - \boldsymbol{\alpha}) = J(\boldsymbol{\sigma} - \boldsymbol{\alpha}) - \sigma_o - R = 0 \tag{2.4}$$

2.1.2 Kinematic Hardening Rule

The Chaboche model for non-linear kinematic hardening in cyclic viscoplasticity model [3] includes:

$$\mathbf{a}_{\mathrm{i}} = \frac{2}{3} C_{\mathrm{i}} \dot{\varepsilon}^{in} - \gamma_{\mathrm{i}} \mathbf{a}_{\mathrm{i}} \dot{p} - b_{\mathrm{j}} J_{a,\mathrm{i}}^{r_{\mathrm{i}}-1} \mathbf{a}_{\mathrm{i}} \tag{2.5}$$

1. First term in (2.5) is the Inelastic linear strain hardening based on Prager, 1949 [9]
2. Second term in (2.5) is the Nonlinear dynamic recovery based on Armstrong-Frederick, 1967 [10]
3. Last term in (2.5) is the Static recovery based on creep modeling of Malini et al., 1972 [11]

Above terms are elaborated in the following section:

Rate Independent Kinematic Hardening

Most of the materials, show tension- compression unsymmetric by a phenomenon called as Bauschinger effect. At the same time during the cyclic loading, the peak stress evolution is such that materials tend to stabilize early without any increase in the yield surface like the isotropic hardening as described in previous section. Such a behaviour is known as Kinematic hardening behaviour.

Numerically, kinematic hardening leads to a shift in the yield surface in the stress space as shown in Figure 2.1, with the aid of an internal variable termed as back stress α. The yield surface takes the form as described in equation 2.6, where α is a back stress tensor.

$$\mathrm{F}(\sigma - \alpha, \mathrm{k}) = 0 \tag{2.6}$$

The back stress is the centre of (or the origin) and plastic loading from f($\sigma(t_1)$) to f($\sigma(t_2)$) results in a change in the backstress and therefore a shift in the yield surface [12].

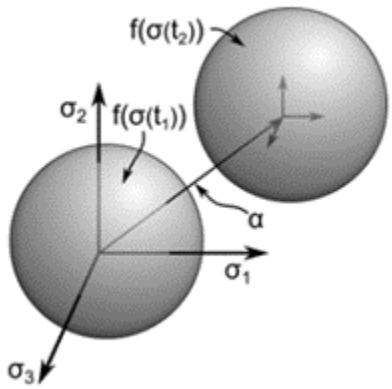

Figure 2.1. Kinematic hardening of the yield surface [12]

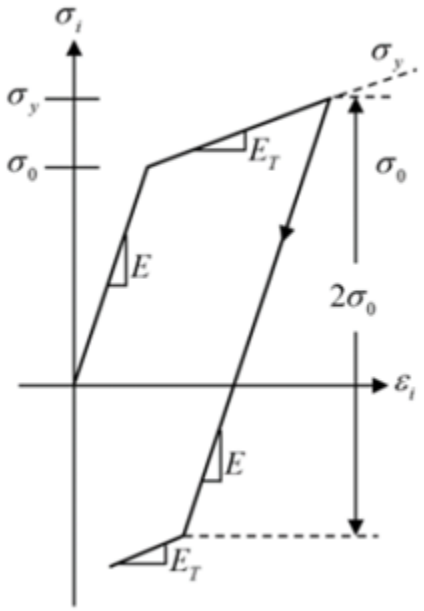

Figure 2.2. Yield stress evolution for Kinematic hardening [12]

The variation of the yield stress upon reversal of load is shown in Figure 2.2, which enable the kinematic hardening model to simulate the Bauschinger effect, in which the centre of the yield surface moves in response to plastic strain increment. Although the variation in stress after yielding as shown in Figure 2.2 is linear, but metallic alloys shows a non-

linear evolution of stress or hardening. Numerically, this non-linear hardening response to plastic strain increment is captured by incrementing back stress (alpha) in correspondence to increment in plastic strain and at the same time making it a function of the current back stress value which makes the curve nonlinear. The Chaboche Kinematic Hardening model is a nonlinear kinematic hardening rule which involves the superposition of several back stress tensor terms , as given in equation 2.7, to descibe the non-linear hardening and realistic shapes of strain-strain curves [12].

$$\alpha = \sum_{\mathrm{i}=1}^{n} \alpha_{\mathrm{i}} \tag{2.7}$$

Where n is the number of kinematic models to be superposed such that the evolution of each back stress model in the superposition in the kinematic hardening rule is given by equation 2.8

$$\dot{\mathbf{a}}_t = \frac{2}{3} C_{\mathrm{i}} \dot{\varepsilon}^{vp} - \gamma_l \mathbf{a}_{\mathrm{i}} \dot{p} \tag{2.8}$$

Where Ci and Yi are materials constants to be calibrated, (symbol eph dot) the plastic strain rate, and (symbol)is the magnitude of the plastic strain increment. The yield criterion is expressed on equation 2.9 as:

$$F = \sqrt{\frac{3}{2}(\mathbf{s} - \boldsymbol{\alpha}) : (\mathbf{s} - \boldsymbol{a})} - R = 0 \tag{2.9}$$

Stress Relaxation

As mentioned in equation 2.5, the last term in the viscoplastic model is the static recovery term. Static recovery provides creep and thermal recovery for low strain rates and high temperatures and the second invariant of the back stress [3] is expressed in following equation as:

$$\dot{\mathbf{a}}_t = \frac{2}{3} C_{\mathrm{i}} \dot{\varepsilon}^{vp} - \gamma_l \mathbf{a}_t \dot{p} - b_r J_{a,t}^{\eta-1} \mathbf{a}_t. \quad J_{a,\mathrm{i}} = \sqrt{\frac{3}{2} \mathbf{a}_{\mathrm{i}} : \mathbf{a}_{\mathrm{i}}} \tag{2.10}$$

In situation where the material is held at constant strain at a temperature greater than 0.4 times the homologous temperature for a period of time, as shown in figure 2.4(a), the stress amplitude decreases gradually with time. This phenomenon is known as Stress relaxation and is depicted in Figure 2.4(b). Plastic deformation occurs because of dislocation motion under the influence of stress. The dislocations further interact and entangle with each other as the plastic deformation progresses, thereby increasing the dislocation density.

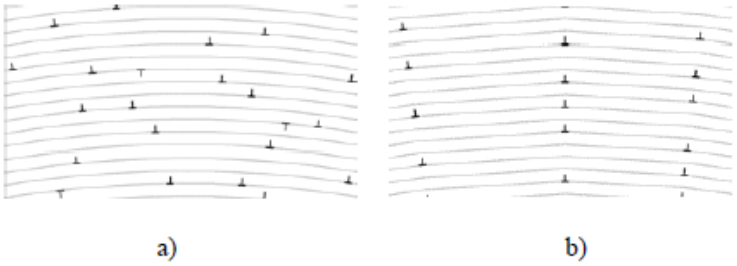

Figure 2.3. a) Annihilation and b) reorganisation of edge dislocations in a crystal lattice [13]

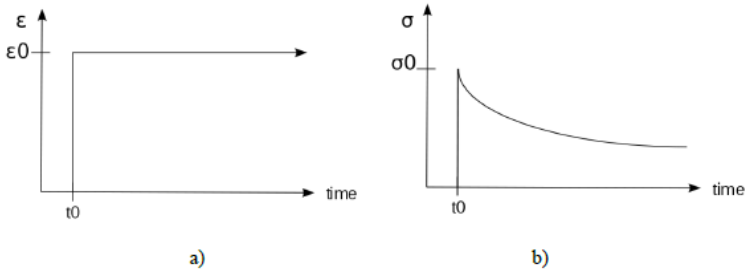

Figure 2.4. Typical Stress relaxation trend during the strain -dwell period. a) Applied strain, b) Induced stress relaxation. [14]

As the temperature increases, the dislocations become mobile and are able to climb, cross slip and glide. When the total strain is constrained during the dwell period in strain control LCFC tests, the dislocations then travel in the opposite directions and cancels each other out by aligning as shown in Figure 2.3. Since each dislocation is associated with stored strain energy which contributes to the material's total strain energy, when two dislocations meet, they essentially cancel out their contribution to the stored energy. This process is called as

dislocation annihilation, which leads to decreased dislocation density and results in recovery and stress relaxation, manifested as the hyperbola function as shown in Figure 2.4.[15]

2.1.3 Formulation of Damage Rule

There is another class of damage model based on the stabilized response which considers a continuous damage evolution during each cycle, called as Incremental lifetime model. Here an ordinary differential equation (ODE) is formulated with respect to internal variables to model the damage evolution during the cycle. The ODE evaluates the change in damage based on the change in the magnitudes of the internal variables for each time increment. Thus, an integration, encompassing each time increment results into the accumulation of damage within the cycle. It is because of this integration procedure, the respective models based on the ODEs in time are denoted as incremental lifetime models.[16]

Like the parametric models, the incremental life rules are especially efficient for those applicable to materials which manifests a stabilized response in initial cycles so that the damage accumulated in a stable cycle (δ D) is considered same for each cycle throughout the loading history until failure. Thus, the overall life span can be approximated by taking the inverse of D ($N_f = 1/$ D). Where the damage variable D, lies in the range $0 <$ D $<$ 1, where D $= 1$ implies the appearance of a technical crack with the order of size of a few millimetres.[16]

The incremental life consumption rule calculates the damage accumulation by time integration along the loading path and therefore accounts for the damaging impact of any loading state. This makes the incremental lifetime rules more advantageous compared to parametric models, since they consider the loading histories so that complex histories like creep-fatigue interaction and multiaxial loading can be evaluated.

In a component under Thermomechanical load, microcracks nucleate in the regions on material imperfections like voids, pores, oxide spikes, dislocation pile ups or interfaces of persistent slip bands. Under cyclic loading these microcrack grow and coalescence together to form a macrocrack (technical crack). It is the cycles required for the growth of these microcrack to form macrocrack that defines the lifetime of the material.

One such incremental damage rules, which is a creep-fatigue damage rate equation is proposed by S. Mujumdar [17]. The damage rate equation takes into account the effect of plastic strain and strain rate, such that the growth of each microcrack from a0 to af is the lifetime mechanism. This damage rate equation is expressed first as crack growth Equation 2.11 which was modified to make Equation 2.11 independent of crack length by introducing a damage parameter D as represented in Equation 2.12

$$\frac{da}{dt} = \dot{a} = Ca \left|\varepsilon_{\text{in}}\right|^{m_1} \left|\dot{\varepsilon}_{\text{in}}\right|^{n_t} \tag{2.11}$$

$$\dot{D} = \frac{C}{\ln\left(a_f/a_0\right)} \left|\varepsilon_{\text{in}}\right|^{m_{\text{i}}} \left|\dot{\varepsilon}_{\text{in}}\right|^{n_{\text{i}}} \tag{2.12}$$

$$D := \frac{\ln\left(a/a_0\right)}{\ln\left(a_f/a_0\right)}, \quad 0 \leq D \leq 1 \tag{2.13}$$

where ϵ and $\dot{\epsilon}$ are the plastic strain and strain rates in the uniaxial case. Equation 2.12 was further modified to replace the Ein by equivalent stress since the effect of creep is more pronounced through introduction of stress and so new form was expressed in [18] as

$$\frac{\mathrm{d}D}{\mathrm{d}t} = \left(\frac{\sigma_{\text{eq}}}{A}\right)^m \left(\frac{\dot{p}}{\dot{p}_0}\right)^n \dot{p}_0 \tag{2.14}$$

where σ_{eq} is the Mises equivalent stress, is the inelastic Mises equivalent strain-rate as defined in Equation 2.14 and $\dot{p_0}$ is a normalisation constant. The material parameters A and m describe the stress-dependence of the lifetime behaviour. The parameter n describes the time-dependence of the lifetime such that for rate-independent behaviour n is equal to 1, whereas n equal to zero means that a fully time dependant behaviour [18]

Further,σ_{eq} in equation 2.14 was replaced by Equivalent Inner Back Stress Xeq to suit the behaviour of Cast Iron [19] as:

$$\dot{D} = \frac{dD}{dt} = \left(\frac{X_{\text{eq}}}{A}\right)^{m_l} \quad \left(\frac{\dot{p}}{\dot{p}_0}\right)^{n_l} \quad \dot{p}_0, \quad X_{\text{eq}} := \sqrt{\frac{3}{2}}\|\mathbf{X}\| \tag{2.15}$$

Equation 2.15 is further integrated over the stabilized cycle to calculate the damage accumulation for the entire cycle which leads to the calculation of Life in number of cycles, as shown below:

$$dD = \left(\frac{X_{aq}}{A}\right)^{m_i} \left(\frac{\dot{p}}{\dot{p}_0}\right)^{n_i} \dot{p}_0 dt \longrightarrow \begin{matrix}\text{Integration over} \\ \text{stabilized eycle} \\ \Delta D\end{matrix} \longrightarrow N_f = \frac{1}{\Delta D} \tag{2.16}$$

Above mention damage rate and incremental lifetime rule has shown fairly good correlation for Ni-Resist D-5S cast iron alloy in response to isothermal and TMF loading [16], as shown in Figure 2.5

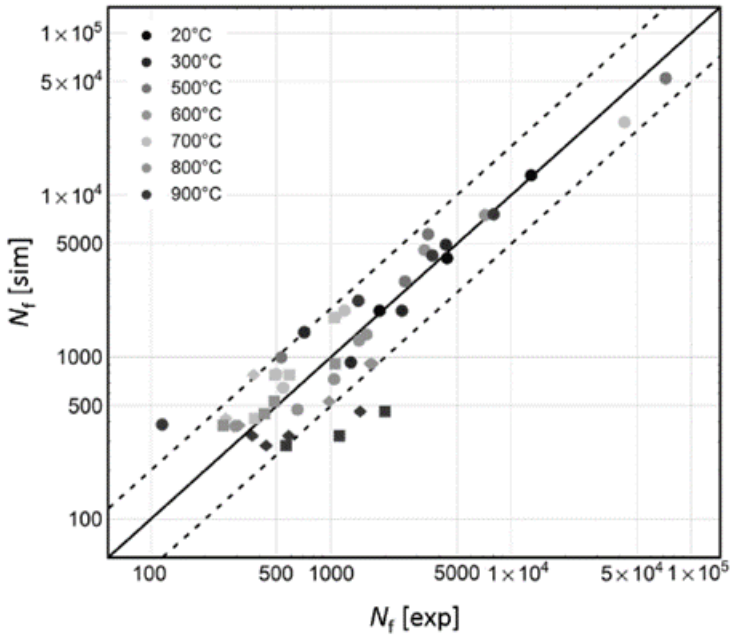

Figure 2.5. Experimental and simulated life correlation using incremental lifetime rule for Ni-Resist D-5S alloy. The filled circles represent LCF tests, the squares represent non-isothermal IP tests and the diamonds show non-isothermal OP tests. The highest temperature of the TMF tests is indicated by the colour [16]

2.1.4 Implementation of Models in FEA

Implementation of Unified Viscoplasticity model in FEA

In presented study, material viscoplasticity and damage modelling are implemented in ANSYS software. In Ansys there are several numerical models present and the Unified Viscoplastic model can be developed by a combination of Kinematic hardening, Perzyna Viscoplastic and Static Recovery models, which are discussed below:

1. The non-linear variation of stress -strain for all the conditions, is appropriately modelled by a non-linear kinematic hardening model for deformation. Thus, chaboche non-linear kinematic hardening model is selected, as shown below in equation 2.17

$$\dot{\boldsymbol{\alpha}}_{\mathrm{i}} = \frac{2}{3} C_{\mathrm{i}} \dot{\hat{\varepsilon}}^{pl} - \gamma_{\mathrm{i}} \dot{\varepsilon}^{pl} \alpha_{\mathrm{i}} + \frac{1}{C_{\mathrm{i}}} \dot{C}_{\mathrm{i}} \alpha_{\mathrm{i}} \tag{2.17}$$

2. To simulate the rate sensitivity, which implies the rate independent regime, can be modelled in Ansys using Perzyna Viscoplastic model expressed in equation 2.18, in combination with equation 2.17

$$\hat{\varepsilon}_{pl} = \sum_{\mathrm{i}=1}^{n} \gamma_{\mathrm{i}} \left(\frac{\sigma}{\sigma_0} - 1 \right)^{1/m_{\mathrm{i}}} \tag{2.18}$$

3. To exhibit stress relaxation behaviour during the dwell period in LCFC tests. This response can be modelled in ANSYS by adding static recovery term (Equation 2.19.) to the back stress rate Equation in 2.17.. Thus, the modified equation becomes:

$$\frac{C_{\mathrm{i}}}{M_{\mathrm{i}} m_{\mathrm{i}}} \left| \alpha_{\mathrm{i}} \right|^{m_{\mathrm{i}}-1} \alpha_{\mathrm{i}} \tag{2.19}$$

$$\dot{\boldsymbol{\alpha}}_{\mathrm{i}} = \frac{2}{3} C_{\mathrm{i}} \dot{\boldsymbol{\varepsilon}}^{pl} - \gamma_{\mathrm{i}} \dot{\varepsilon}^{pl} \boldsymbol{\alpha}_{\mathrm{i}} + \frac{1}{C_{\mathrm{i}}} \dot{C}_{\mathrm{i}} \boldsymbol{\alpha}_{\mathrm{i}} - \frac{C_{\mathrm{i}}}{M_{\mathrm{i}}^{m_{\mathrm{i}}}} \bar{\alpha}_{\mathrm{i}}^{m_{\Gamma}-1} \boldsymbol{\alpha}_{\mathrm{i}} \tag{2.20}$$

Thus, with combination of Equation 2.18 and Equation 2.20, a unified viscoplastic material model combination is capable to simulate strain-rate effect and stress relation behaviour.

2.1.5 Implementation of Damage Model in FEA

The incremental lifetime rule as described in section 2.2 is implemented using Ansys Customisation Tool kit as shown in figure 2.6

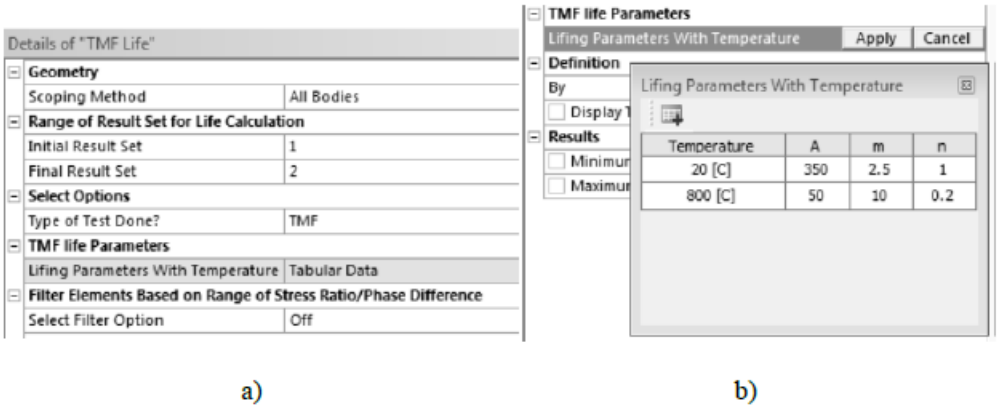

Figure 2.6. Damage model interface in Ansys

3. APPLICATION OF THE DAMAGE MODEL FOR FATIGUE LIFE PREDICTION

Presented case study is based upon the implementation of unified viscoplasticity theory as discussed in chapter 2 to model the deformation of SiMo4.06 Ductile Cast Iron in response to isothermal LCF and TMF loads, and implementation of incremental lifetime rule as mentioned in section 2.2 to predict isothermal LCF life in FEA software.

3.1 Material Characterisation

Cast irons are ferrous alloys that contains more than 2% wt. carbon. There are three type of cast irons in general as grey iron, compacted graphite cast iron and ductile cast iron. These cast irons are classified according to their graphite shape as shown in Figure 3.1.

SiMo is a group of ferritic ductile cast irons alloyed with Si and Mo. Ferritic cast iron materials are often used for high temperature applications like the exhaust manifolds, turbine housing, cylinder head and block because of low costs, high heat conductivity and low coefficient of thermal expansion compared to austenitic materials [6].

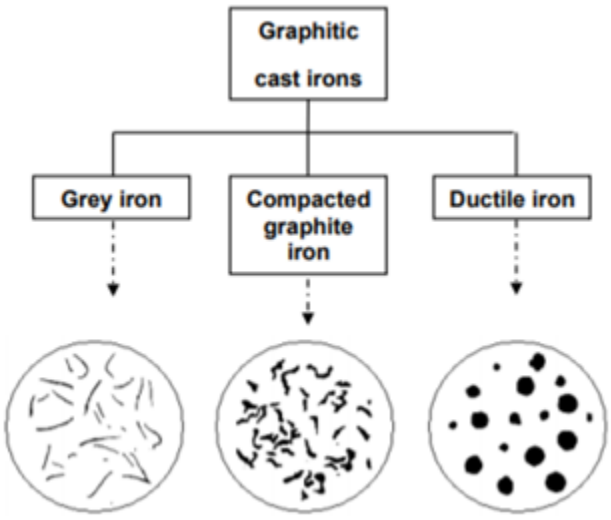

Figure 3.1. Morphologies of different graphitic cast irons, such as grey iron, compacted graphite iron and ductile iron [20]

Microstructure Analysis

SiMo4.06 (Fe-3.2C-4.0Si-0.6Mo) consists of uniformly distributed graphite nodules and Mo-rich eutectic phases formed in cellular structure. The shape of these nodules (dark) is spherical, and its diameter varies from 10 μm to 30 μm. The eutectic cell (diffuse grey) is close to 100 μm, and the thickness of the eutectic segments Figure 3.2 is about 2 μm in thickness, distributed along grain boundaries [21]. The microstructure of the DCI is shown in the Figure 3.2 below.

The silicon and molybdenum content raises the oxidation resistance, the stability of the ferritic matrix and the creep strength at high temperatures in comparison with unalloyed grey irons [22]

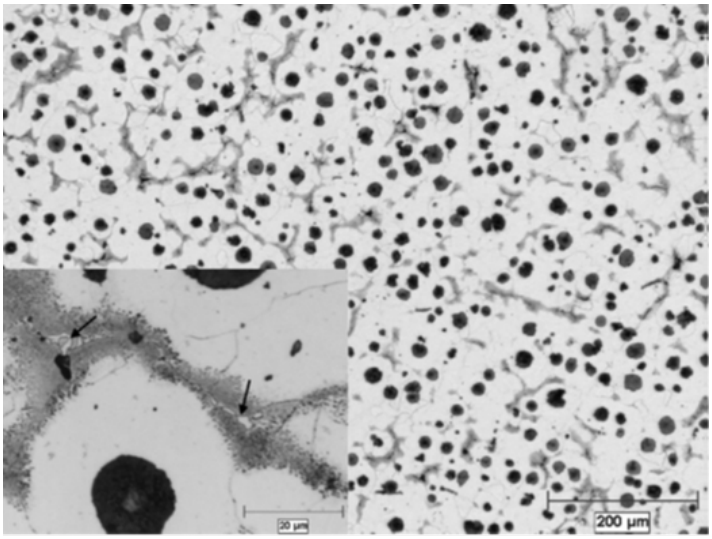

Figure 3.2. Optical micrographs of high Silicon (Fe-3.2C-4.0Si-0.6Mo) SiMo4.06 DCI with the cell boundaries (diffuse grey contrast around) resolved by etching. The arrows indicate the Mo-rich eutectic primary carbide phase [21]

Chemical, Mechanical and Thermophysical Properties of SiMo4.06

The chemical composition of the Ductile Cast Iron is mentioned in the Table 3.1. This composition of DCI also referred to as SiMo4.06 Cast Iron.

Table 3.1. Nominal Chemical Compositions of the Tested Materials (Weight Percent) [21], [22]

Si	C	Mo	Mn	Cr	Cu	Mg	P	Ni	AL
4.10	3.21	0.55	0.394	0.085	0.066	0.048	0.038	0.024	0.018

Mechanical and thermophysical properties are essential to obtain so as to conduct the steady state (isothermal) and transient thermal simulations using the numerical model. The temperature dependant physical properties such coefficient of thermal expansion, thermal conductivity, specific heat, and density are depicted in Figure 3.3. Additionally, temperature dependant young's modulus and yield strength, as shown in Figure 3.4, are obtained from the report [23].

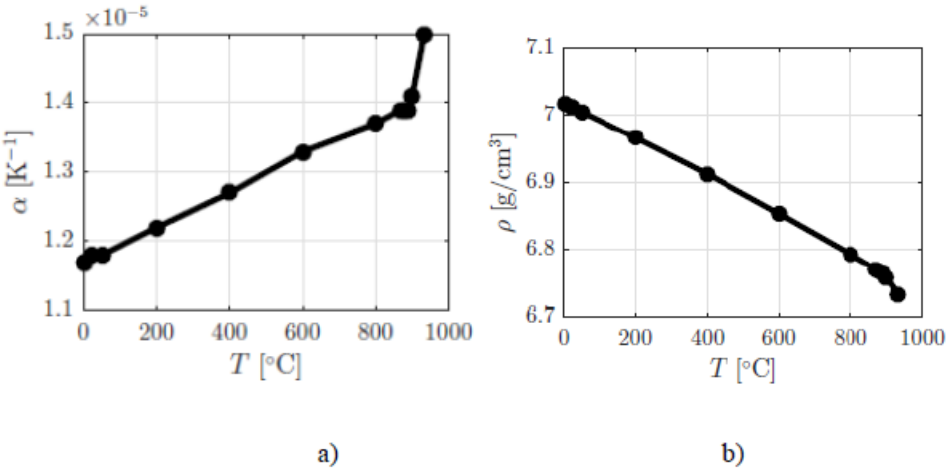

Figure 3.3. Coefficient of (a) thermal expansion, (b) density, [24]

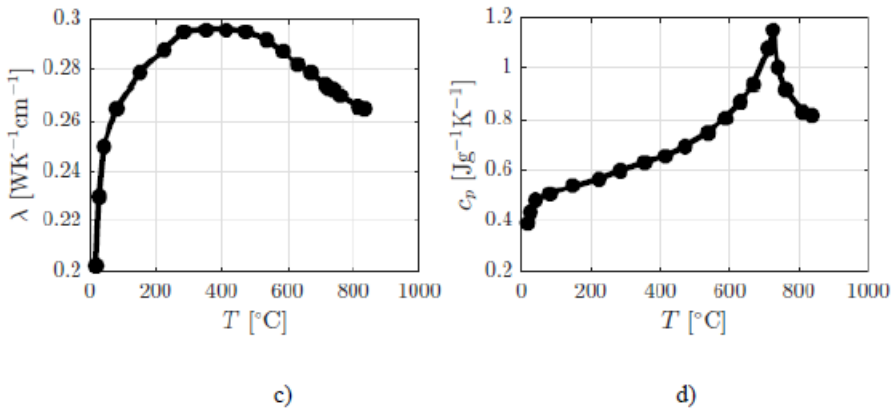

Figure 3.4. (c) thermal conductivity, (d) specific heat, [24]

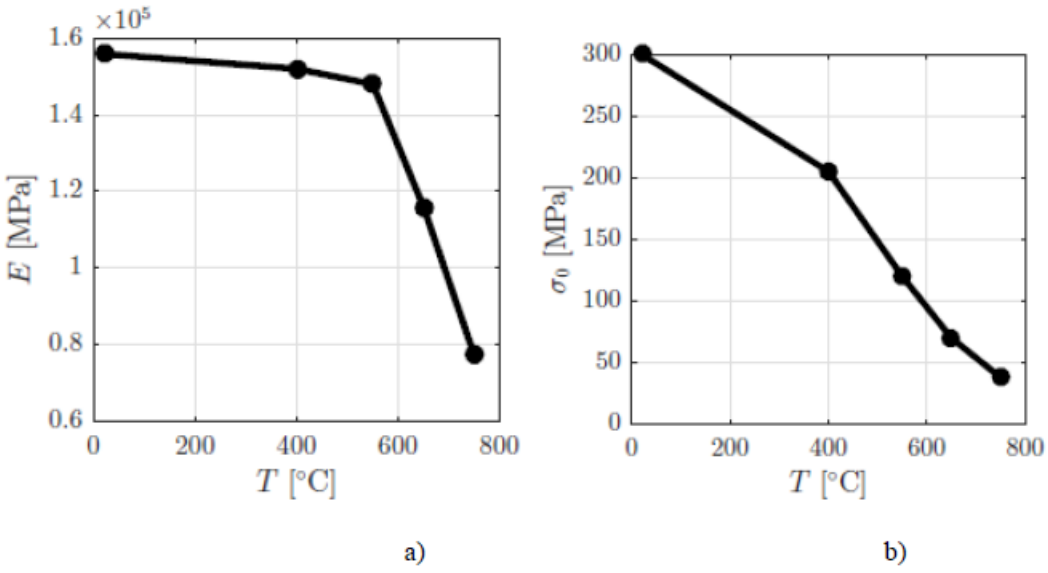

Figure 3.5. (a)Young's modulus and (b)Yield Strength [24]

3.2 Finite Element Model

FEA is conducted using a single element model as shown in Figure 3.6, 3.7. A uniaxial loading case is simulated where three sides of the element, (sides normal to each axis) are applied Roller support, called as Frictionless support in Ansys. As a thermal loading, temperature is applied over the face normal to y-axis as per the test conditions.

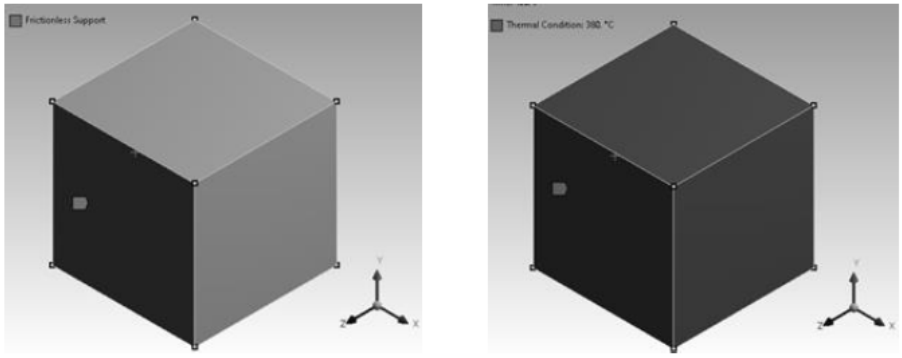

a) b)

Figure 3.6. Single Element FEA model: a) frictionless support, b) body temperature

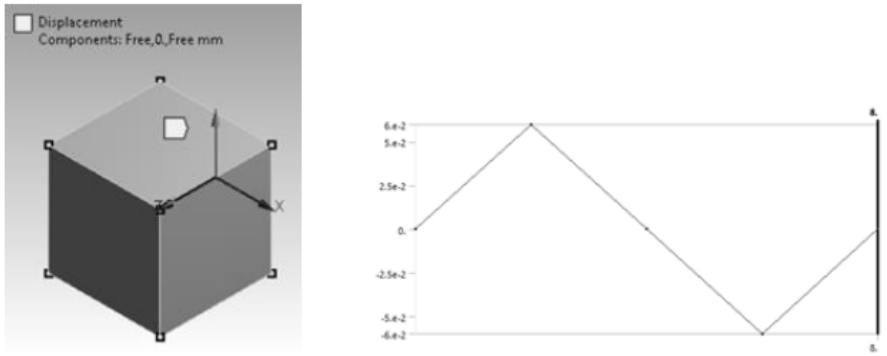

c) d)

Figure 3.7. Single Element FEA model: c) displacement in y-direction, d) Temperature profile

3.3 Testing Conditions

To characterise SiMo4.06 material's response to thermomechanical loads and dependency on parameters like temperature, strain rate and hold time, various isothermal LCF and LCFC experiments were conducted by M. Bartosak [25] and TMF experiments were conducted by Wu [26], which are mentioned as follows:

Isothermal Low Cycle Fatigue (LCF) test - Without holdtime

1. Strain rate: 0.003/s + Strain amplitude = 0.006
   (a) T = 20°C
   (b) T = 400°C
   (c) T = 550°C
   (d) T = 650°C
2. Strain rate: 0.00001/s + Strain amplitude = 0.006
   (a) T = 400°C
   (b) T = 550°C
   (c) T = 650°C
3. Strain rate: 0.0001/s + Strain amplitude = 0.006
   (a) T = 550°C

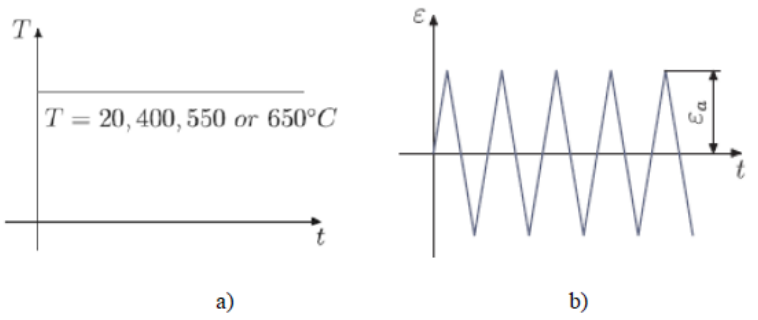

Figure 3.8. Strain controlled LCF test loads: a) Temperature history, b) strain history [25]

Isothermal LCF-Creep test, With holdtime (th) of 300 seconds:

1. Strain rate: 0.003/s + Strain amplitude = 0.006

   (a) T = 400°C

   (b) T = 550°C

   (c) T = 650°C

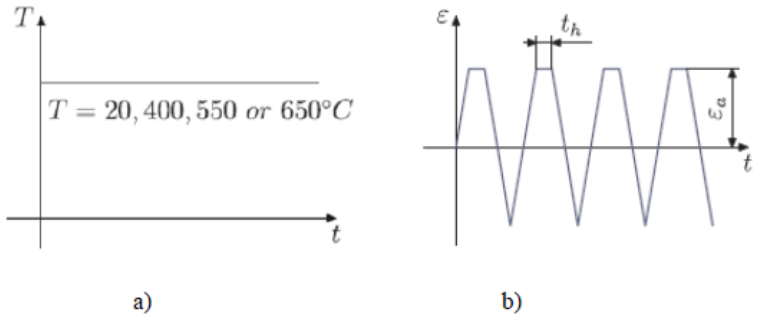

Figure 3.9. Strain controlled LCF-Creep test loads: a) Temperature history, b) strain history [25]

Constrained Thermomechanical Fatigue (TMF) Test

The TMF tests were conducted in accordance with ASTM E2368, with a minimum temperature of 160°C and maximum temperature of 600°C. In this test, the mean temperature

was 380°C and thermal strain equation was determined such that thermal strain was set zero under zero load for the DCI and offset [26] at 380°C as shown in following Figure 3.10

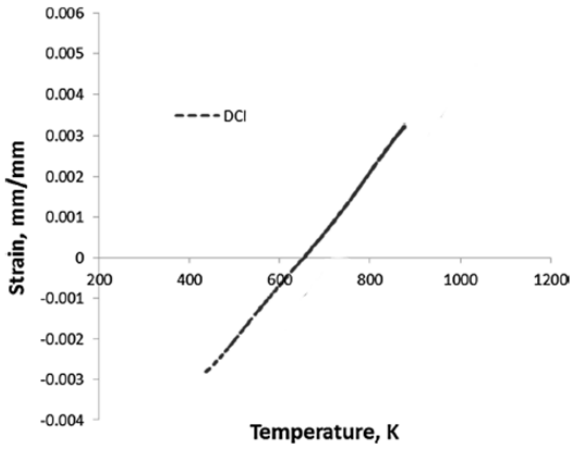

Figure 3.10. Thermal expansion curves offset at 380°C (653 K) [26]

Then a constrain ratio was established as per equation 3.1. and TMF test were conducted at three constrained ratio conditions: 100%

$$\eta = \frac{\varepsilon_{\text{th}} - \varepsilon_{\text{t}}}{\varepsilon_{\text{th}}} \tag{3.1}$$

For each of the constrained ratio test, the temperature profile with which TMF tests are performed is shown in Figure 3.9.

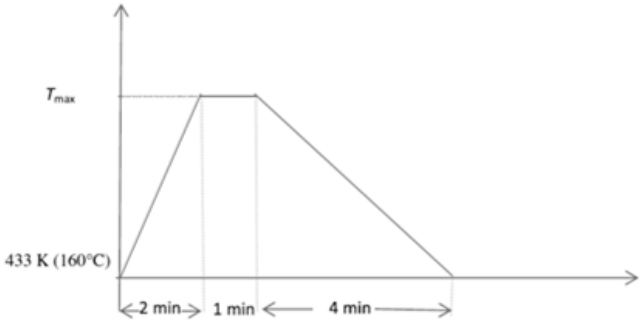

Figure 3.11. Temperature profile and cycle time for constrained TMF test [26]

4. RESULTS AND DISCUSSION

4.1 Parameter Estimation for Unified Viscoplastic Model

The most important steps after the selection of the material models to be implemented to model the deformations, is the parameter estimation. The chosen material model in Equation 2.18 and Equation 2.20 has several constants to be determined along with the Yield strength and Young's modulus.

Thus, a procedure is followed to determine the constants for the unified viscoplastic model as per [3], which is described below:

1. Determine the Young's modulus and yield strength from the stabilized hysteresis loop for each temperature

2. Estimate initial parameters for the chaboche rate independent non-linear kinematic hardening model without static recovery at highest available strain rate. Calibrate the parameters

3. Use the values of chaboche constants calibrated in step-2 as initial estimate for unified viscoplasticity model. Include the hysteresis data of all available strain-rates for Perzyna model parameter determination and include stress relaxation data for each temperature to determine constants for static recovery term in chaboche model

4.1.1 Determination of Young's Modulus and Initial Yield Stress

The Young's Modulus is determined by taking the slope of the linear region in the hysteresis loop, as shown in Figure 4.1. First, by subtracting the elastic strain from the total strain, a plot of plastic stain vs stress (as shown in Figure 4.1, second can be obtained from which yield stress value is determined.

Thus, yield strength and Young's modulus for all the temperatures are calculated and mentioned in Table 1 below:

Table 4.1. Calculated temperature dependent Young's modulus (E) and Yield stress (YTS)

(T ^{0}C)	E (Mpa)	YTS (Mpa)
20	142390.24	253.5
400	143221.79	196.47
550	136967.88	65.97
650	121134.62	27.01

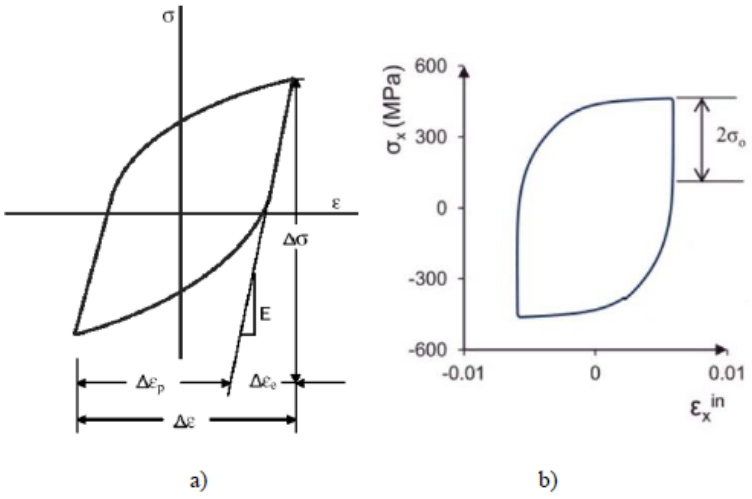

Figure 4.1. a) Strain partitioning of hysteresis loop, b) Typical plot of inelastic strain vs stress [27]

4.1.2 Parameter Estimation of Chaboche Nonlinear Kinematic Hardening Model

The initial parameters for the chaboche model are determined from stabilized hysteresis loop experimental data obtained at each temperature. To accurately model the complex deformation, a third order chaboche model is considered with 3 back stress terms as per the Equation 4.1.

$$\frac{C_1}{\gamma_1} + \frac{C_2}{\gamma_2} + \sigma_0 = \sigma_x - \frac{C_3}{2}\left(\varepsilon_X^{pl} - \left(-\varepsilon_L^{pl}\right)\right) \tag{4.1}$$

Thus, the hysteresis loop can be divided into 3 regions as shown in Figure 4.2. Part 1 is the initial onset of yielding, Part 2 is the knee of the hysteresis curve, and Part 3 is the constant modulus segment.

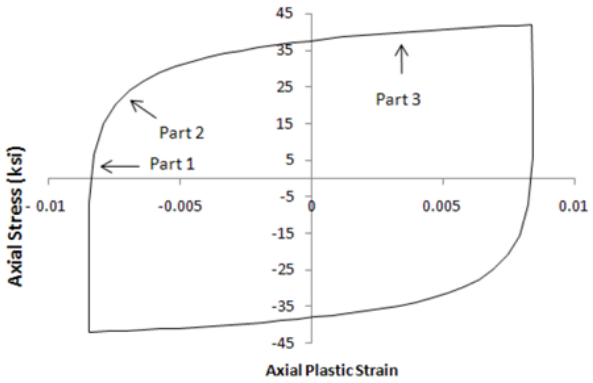

Figure 4.2. Partitioning of hysteresis loop for Chaboche model [28]

Using the described heuristic method, the initial material parameters can be estimated as follows:

1. σ_o is the initial yield stress of the material
2. C1 in equation 4.1 is the slope in Part 1 of the stress-strain curve at the transition from elastic to plastic deformation. This value is approximately the plastic modulus at yielding
3. Using equation 4.1, Y1 should be large enough that the exponential term quickly diminishes so that α is approximately constant outside of Part 1
4. C2 is chosen as a slope from Part 2
5. Y2 is calculated from the chosen C2 and the ratio C2/Y2 such that it satisfies Equation 4.1
6. C3 is the slope of the stress-strain curve in Part 3
7. Y3 is not included in equation 4.1 and is assigned a small positive value

Once the initial parameters are estimated, a non-linear regression procedure is followed to determine the material parameters that minimize the error between data and model parameter to obtain fairly good curve fit for all the experiments.

Table 4.2. The calibrated constants for all the temperatures for the viscoplastic model

Parameters	(20°C)	(400°C)	(550°C)	(650°C)
C1	0	0.22	0.63	0.73
C2	0	0.18	0	0.00
C3	253.5	196.47	65.98	27.01
C4	14499119.16	344167.14	87603.13	2868021.34
C5	768462.31	3649.93	1172.73	26079.05
C6	336854.42	93762.82	16698190.78	32424.74
C7	2066.04	710.68	152176.62	1151.50
C8	39065.23	59.3	395.37	0.18
C9	10	0	0	0.00
C10	0	452.84	298172529.3	89480.43
C11	0	7.73	1	1.24
C12	0	2272.07	5504707.3	104488.60
C13	0	4.77	1	1.73
C14	0	4092.09	58090195.68	9808.29
C15	0	1.66	1	1.50

4.2 FEA Model Response Correlation With Experimental Tests

A single element Finite Element Analysis is performed in Ansys software to simulate the stress-strain response to Isothermal LCF, LCFC and TMF tests, The FE results for these tests are correlated with experimental tests and discussed in the following sections.

4.2.1 Isothermal LCF Test: $\mathbf{T = 20°C}$, $\dot{\epsilon} = \mathbf{0.003/s}$

Figure 4.3 represents the Stress-Strain hysteresis loops at midlife, where the data in orange colour represents experimental data points and blue trend represent simulated FEA result points. It can be seen from the figure below that the simulated FEA results correlated well with experimental data at midlife. From [25] SiMo4.06 exhibits rate-independent behaviour at room temperature (20°C) and therefore to numerically achieve this in a same

set of governing viscoplastic equations, the viscosity parameter C2 in Perzyna Viscoplastic model was assigned a very high value and strain rate hardening parameter C1 was assigned zero. This is because, as C2 approaches infinity, the strain rate hardening parameter C1 approaches zero for the Perzyna viscoplastic model as given in Equation 2.18 and the solution thus approaches static rate independent solution. This test result is in accordance with section 4.2, (1.a.i) and figure 3.8 represents the schematic of the loading conditions.

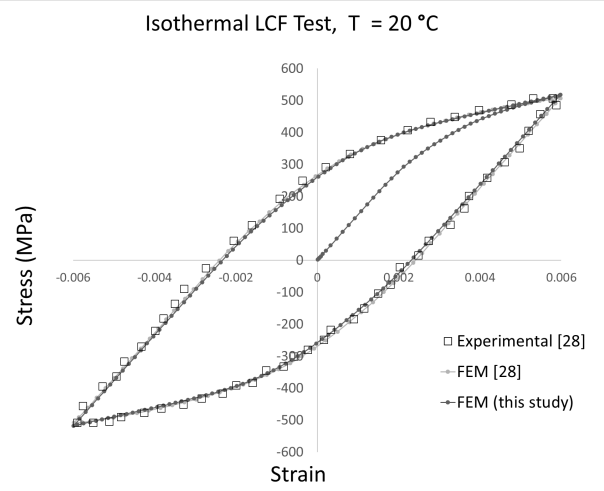

Figure 4.3. Stress-Strain Hysteresis comparison of Experimental [22], FEM [22], FEM (this study) at Isothermal 20°C LCF Test, 0.003/s

4.2.2 Isothermal LCF Test: T = 400°C, $\dot{\epsilon}$ = 0.003/s & 0.00001/s

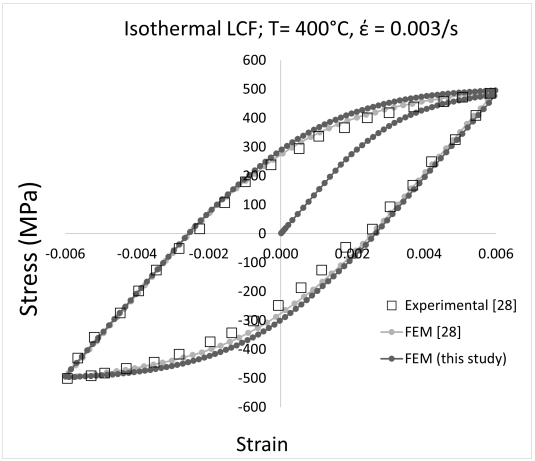

Figure 4.4. Stress-Strain Hysteresis comparison of Experimental [22], FEM [22], FEM (this study) at Isothermal 400°C LCF Test, 0.003/s

Figure 4.4, and 4.5 represents the Stress-Strain hysteresis loops at midlife for the above-mentioned test condition. This particular LCF test was done at 400°C and at this temperature and on wards SiMo4.06 shows rate sensitive behaviour [25] therefore a unique response of the material is observed at each strain rate. Figure 4.6 shows the comparison of simulated hysteresis loop at 0.003/s and 0.00001/s for the above loading conditions. The model parameters derived from calibration techniques resulted to a fairly good correlation of the FEA results with experimental observations at both the strain rates as shown in 4.4, and 4.5. Thus, the model is able to simulate the strain-rate hardening effect well and can be seen in Figure 4.6, where higher strain rate (0.003/s) resulted to increased peak stress.

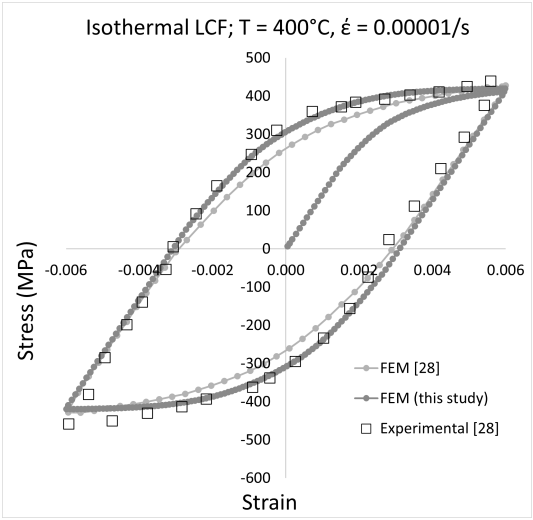

Figure 4.5. Stress-Strain Hysteresis comparison of Experimental [22], FEM [22], FEM (this study) at Isothermal 400°C LCF Test, 0.00001/s

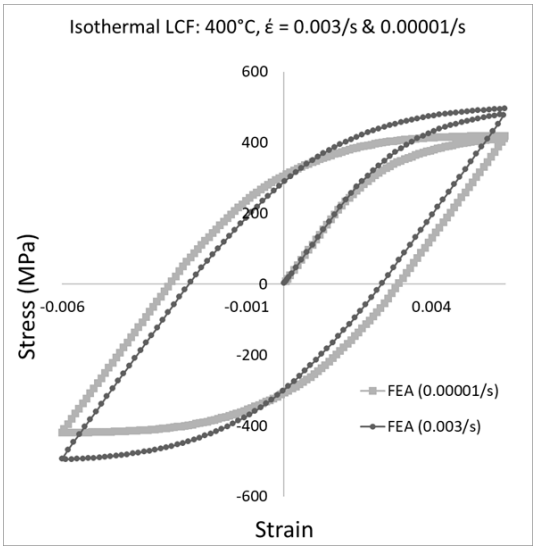

Figure 4.6. FEA correlation for Isothermal LCF at 400°C, 0.003/s and 0.00001/s [25]

This test result is in accordance with section 4.2, (1.a.ii) and (1.b.i) and figure 3.6 represents the schematic of the loading condition.

4.2.3 Isothermal LCF test: T = 550°C, $\dot{\epsilon}$ = 0.003/s, 0.0001/s & 0.00001/s

Figure 4.7 to 4.11 represents the Stress-Strain hysteresis loops at midlife for the above-mentioned test conditions. As mentioned in previous result discussion, SiMo4.06 above 400°C shows rate dependant behaviour. Thus at550°C, the strain rate dependent hardening is simulated well and figure 4.7 demonstrates the simulated strain rate dependent behaviour at 0.003/s, 0.0001/s and 0.00001/s strain rates.

For model parameter estimation, it was required that the model be able to simulate strain-rate dependency along with stress-relaxation and therefore experimental data involved data at 0.003/s, 0.0001/s & 0.00001/s and stress relaxation data during the holdtime. The model FEA predicted deformations are fairly good when compared to experimental analysis. It is observed that the model parameters correlate the maximum and minimum peak stress well, and marginally overpredicts the behaviour after the onset of yielding in both tension and compression at 0.003/s strain rate as shown in Figure 4.9

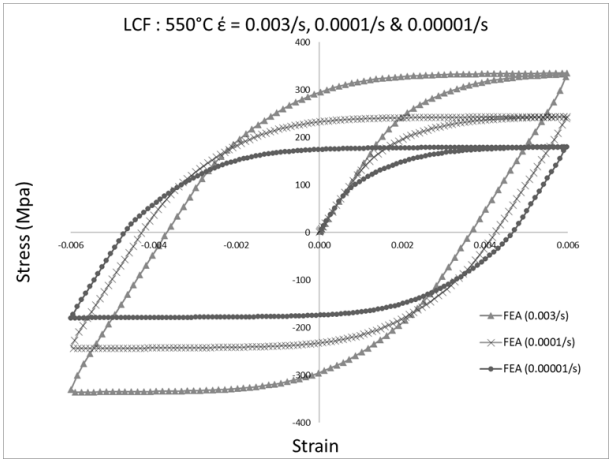

Figure 4.7. FEA Hysteresis comparison at Isothermal LCF at 550°C, 0.003/s,0.0001 and 0.00001/s [25]

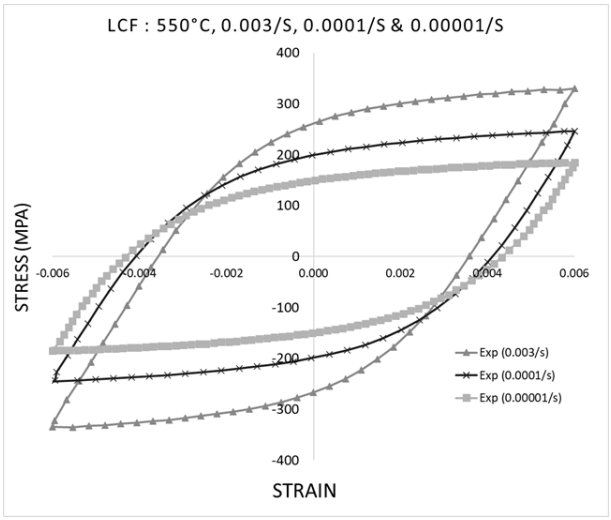

Figure 4.8. Experimental Hysteresis comparison at Isothermal LCF at 550°C, 0.003/s,0.0001/s and 0.00001/s [25]

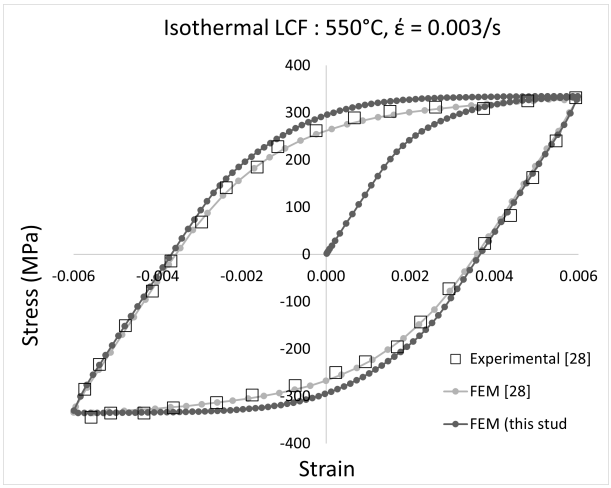

Figure 4.9. Stress-Strain Hysteresis comparison of Experimental [22], FEM [22], FEM (this study) at Isothermal 550°C LCF Test, 0.003/s

The predicted deformation at 0.0001/s and 0.00001/s in figure 4.10 and figure 4.11, shows more variation in stress along the region after the onset of yielding in both tension and compression compared to 0.003/s.

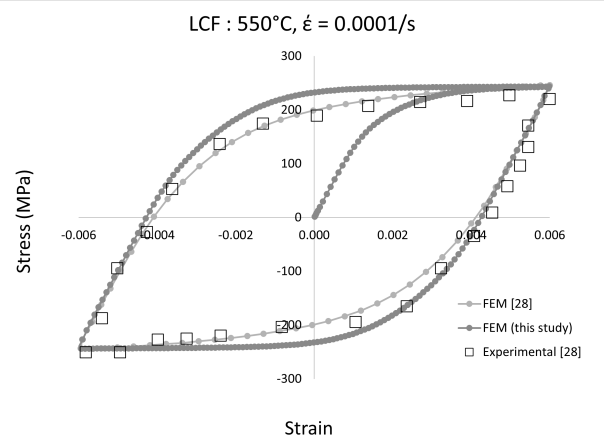

Figure 4.10. Stress-Strain Hysteresis comparison of Experimental [22], FEM [22], FEM (this study) at Isothermal 400°C LCF Test, 0.0001/s

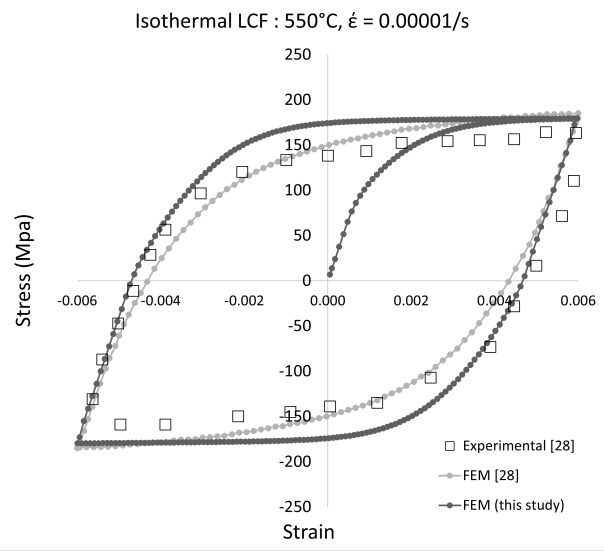

Figure 4.11. Stress-Strain Hysteresis comparison of Experimental [22], FEM [22], FEM (this study) at Isothermal 400°C LCF Test, 0.00001/s

This variation may be attributed due the declining slope of the stress strain curve as strain rate is decreasing as shown in figure 4.8. This test result is in accordance with section 4.2, (1.a.iii), (1.b.ii), (1,c,i) and figure 3.8 represents the schematic of the loading condition.

4.2.4 Isothermal LCF Test: T = 650°C, $\dot{\epsilon}$ = 0.003/s and 0.00001/s

Figure 4.12 and 4.13 represents the Stress-Strain hysteresis loops at midlife for the above-mentioned test condition. As shown in following figure, the slope of strain hardening after the onset of yielding is comparatively low and this can be attributed to the more mobile (less viscous) nature of SiMo4.06 at 650°C. The FEA results shows a good match with the peak stresses at each reversal and overpredicts the stresses after the onset of yielding. This is because, during the calibration, LCF test data at 0.003/s, 0.000001/s and stress relaxation data was utilised to obtain all the model parameters, where the peak stress of 70 Mpa at 0.000001/s were close to the yield strength of 67 Mpa which resulted to a steep slope after the onset of yielding for all the conditions. This test result is in accordance with section 4.2, (1.a.iv), (1.b.iii) and figure 3.6 represents the schematic of the loading condition

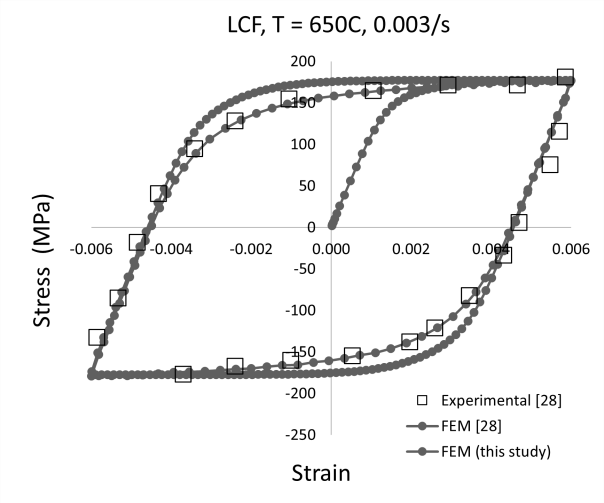

Figure 4.12. Stress-Strain Hysteresis comparison of Experimental [22], FEM [22], FEM (this study) at Isothermal 650°C LCF Test, 0.003/s

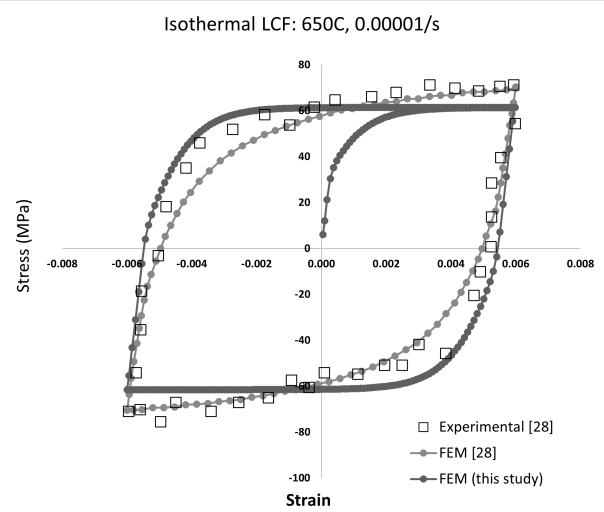

Figure 4.13. Stress-Strain Hysteresis comparison of Experimental [22], FEM [22], FEM (this study) at Isothermal 650°C LCF Test, 0.00001/s

4.2.5 Isothermal LCFC Test,T = 400°C, T_h = 300s, $\dot{\epsilon}$ = 0.003/s

As discussed before, SiMo4.06 shows rate dependency at and above 400°C and so the isothermal LCF tests in previous sections helped to characterise the rate-dependant hardening behaviour. In addition to the LCF tests, a hold time of 300 seconds was introduced to characterise the stress relaxation behaviour.

Figure 4.14 and 4.15 represents the hysteresis response to isothermal LCF-Creep test at 400°C. The vertical trend where the stress decreases at constant strain (at 0.006), represents the response during the hold time. Since the holdtime is introduced in tension, the stress relaxation trend is observed likewise at the end of first monotonic loading.

The model FEA response correlates well with the experimental observations and interestingly the stress relaxation trend during the hold time also shows a good correlation as shown. This test result is in accordance with section 4.2, (2.a.i) and figure 3.9 represents the schematic of the loading conditions

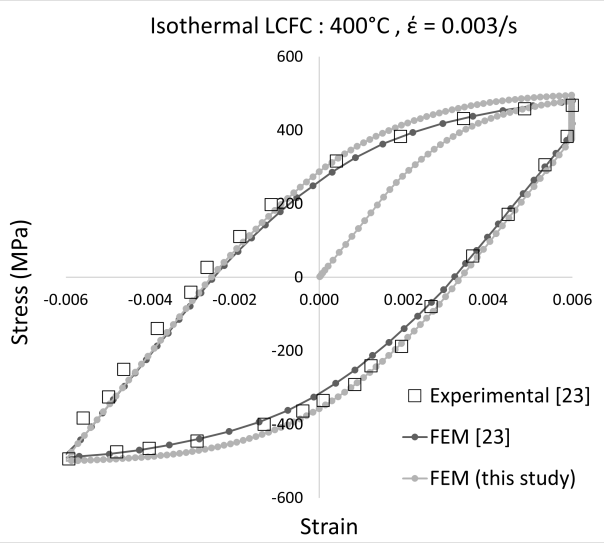

Figure 4.14. Stress-Strain Hysteresis comparison of Experimental [25], FEM [25], FEM (this study) at Isothermal 400°C LCF-Creep Test, 0.003/s

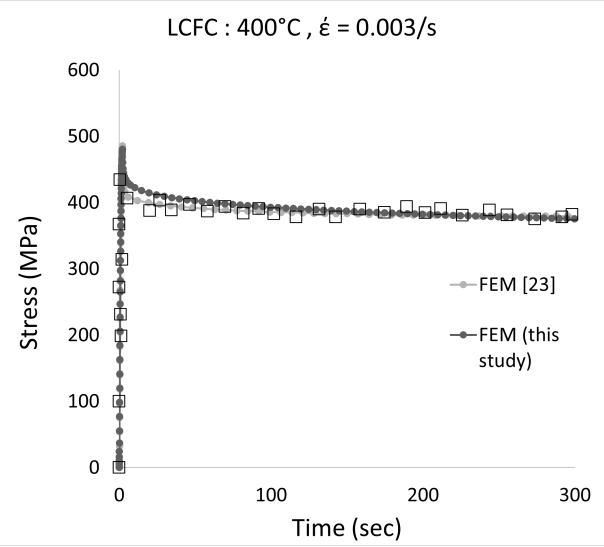

Figure 4.15. Stress Relaxation comparison of Experimental [25], FEM [25], FEM (this study) at Isothermal 400°C LCF-Creep Test, 0.003/s

4.2.6 Isothermal LCFC Test,T = 550°C, T_h = 300s, $\dot{\epsilon}$ = 0.003/s

Figrure 4.16 and 4.17 represents the FEA simulation LCF-Creep response of SiMo4.06 at 550°C. The simulated FEA data shows a good correlation with experimental observations.

The viscoplasticity model requires addition of a static recovery term and looking at the correlation of FEA the parameter estimation can be concluded to be fairly accurate.

As seen in following figures, the stress relaxation has been simulated acculrately and as a result the hysteresis loop correlated well with experimental data.

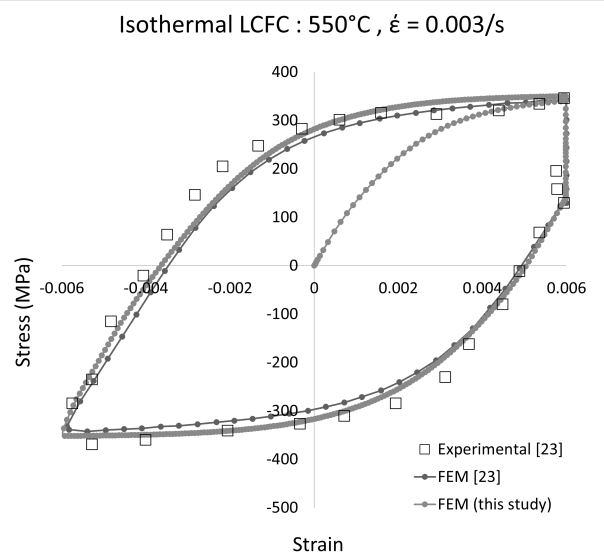

Figure 4.16. Stress-Strain Hysteresis comparison of Experimental [25], FEM [25], FEM (this study) at Isothermal 550°C LCF-Creep Test, 0.003/s

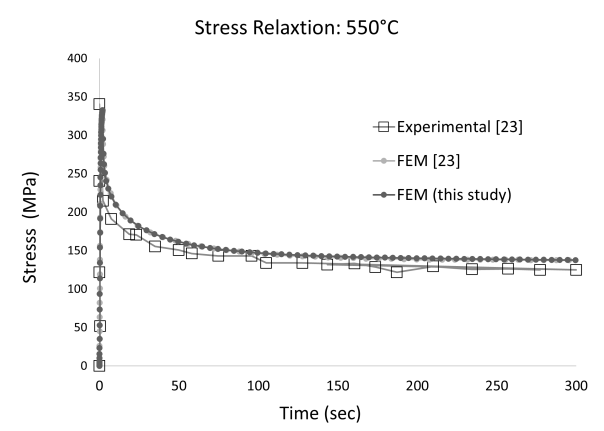

Figure 4.17. Stress Relaxation comparison of Experimental [25], FEM [25], FEM (this study) at Isothermal 550°C LCF-Creep Test, 0.003/s

Further it can be noticed that the relaxed stress is more at 550°C compared to 400°C, which can be related to increase annihilation during the stress relaxation with increasing temperatures. This test result is in accordance with section 4.2, (2.a.ii) and figure 3.9 represents the schematic of the loading conditions.

4.2.7 Isothermal LCFC Test,T = 650°C, T_h = 300s, $\dot{\epsilon}$ = 0.003/s

The FEA simulation response to LCFC at 650°C is shown below. Figure 4.18 represents the stress strain hysteresis loop showing stress relaxation while the strain is constant during the hold time of 300 seconds. The model parameters lead to fairly accurate stress relaxation simulation as shown in Figure 4.19. A good correlation of stress relaxation led to good correlation of stress-strain hysteresis loop as shown in following figures.

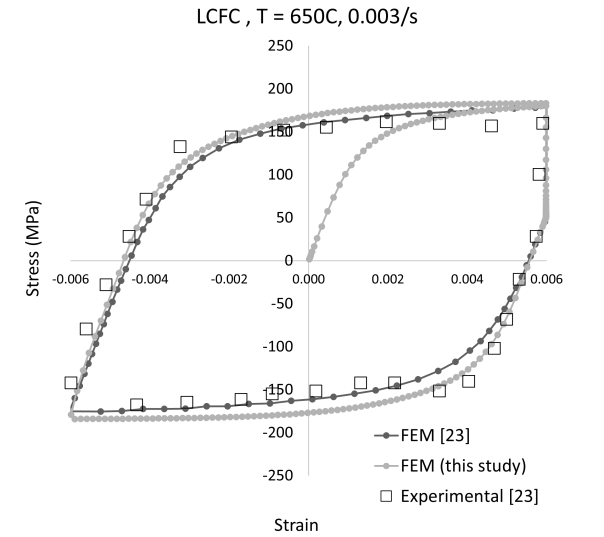

Figure 4.18. Stress-Strain Hysteresis comparison of Experimental [25], FEM [25], FEM (this study) at Isothermal 650°C LCF-Creep Test, 0.003/s

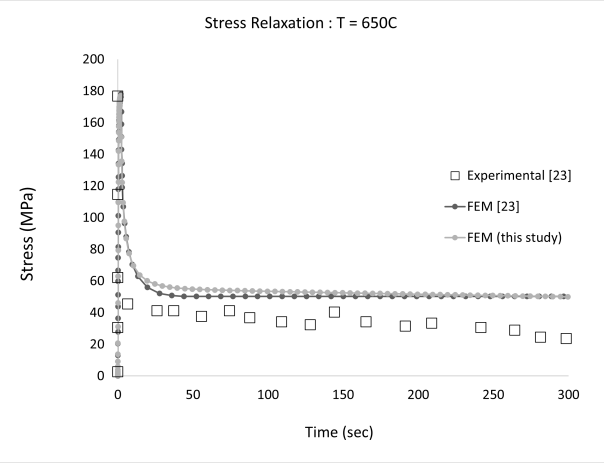

Figure 4.19. Stress Relaxation comparison of Experimental [25], FEM [25], FEM (this study) at Isothermal 650°C LCF-Creep Test, 0.003/s

It is interesting to note that the relaxed stress is below half the peak stress at 650°C and this trend of increased relaxed stress as the temperature increases has been observed consistently from 400°C to 650°C. At 400°C, referring to figure 4.17 the relaxed stress is close to the peak stress while at 550°C the relaxed stress is close to half the peak stress and at 650°C the relaxed stress is beyond half the peak stress which demonstrates the phenomenon of increasing annihilation at higher temperature. This test result is in accordance with section 4.2, (2.a.iii) and figure 3.9 represents the schematic of the loading conditions.

4.2.8 Constrained Thermomechanical Fatigue (TMF) FEA Results

The constrained TMF simulation correlation is the result of cumulative fairly accurate FEA correlation with experiments at all the isothermal temperature LCF and LCFC test conditions as discussed in previous sections. The deformation hysteresis trend is obtained non-isothermal temperature (Tmin = 160°C and Tmax = 650°C) fully constraining the FE model so that the mechanical strains are equal in magnitude and opposite in direction to thermal strain also known as out-of-phase (100 percent)TMF.

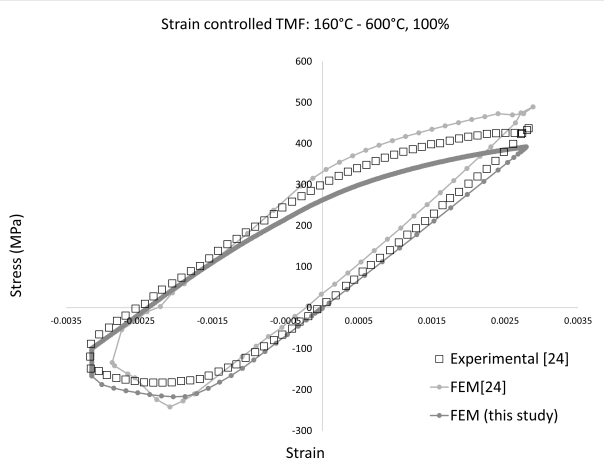

Figure 4.20. Stress-Strain Hysteresis comparison of Experimental [26], FEM [26], FEM (this study) for Constrained (100 %) TMF Test

The model parameters have simulated the hysteresis loop with hold time with good correlation with experimental midlife loop, as shown in figure 4.20. It can be seen that the model deformation varies in the region after the holding time is completed in the first quadrant. Now, it is important to verify the inelastic strain to ensure that the TMF simulation correlates well. Following figure shows a good correlation of FEA and experimental inelastic strains. This test result is in accordance with section 4.2, (3), equation 3.1 represents the mechanical constrain condition and figure 3.11 represents the schematic of the temperature profile.

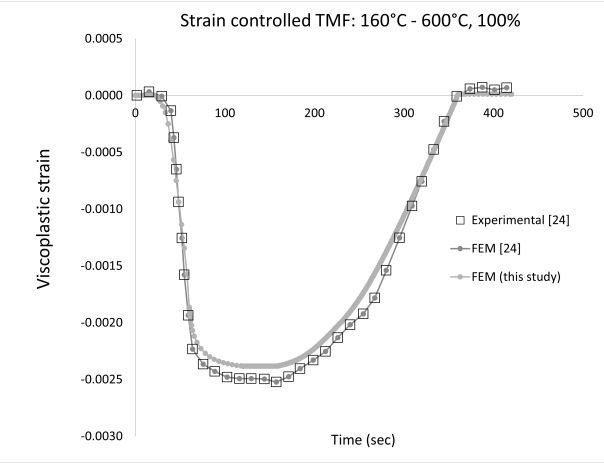

Figure 4.21. Total Inelastic strain comparison of Experimental [26], FEM [26], FEM (this study) for Constrained (100 %) TMF Test

4.3 Parameter Estimation for Damage Rate Model

The damage rate equation consists of three main parameters A, m and n as shown in equation below:

$$\dot{D} = \frac{dD}{dt} = \left(\frac{X_{\text{eq}}}{A}\right)^{m_l} \quad \left(\frac{\dot{p}}{\dot{p}_0}\right)^{n_l} \quad \dot{p}_0, \quad X_{eq} := \sqrt{\frac{3}{2}}\|\mathbf{X}\| \tag{4.2}$$

As per Mujumdar, [17] the parameter n is sensitive to strain rate and it varies within 0 and 1, where n = 1 means rate independent. This value of n can be calculated from log-log plot of strain rate and time to failure and should be plotted for both the tensile and creep test. Following [17], a log-log plot for LCF tensile failure rate is plotted as shown in 4.22, and the parameter is estimated as in table 3. These estimated parameters are helpful to find the final after the least square error minimization method.

Table 4.3. Calculated temperature dependent Young's modulus (E) and Yield stress (YTS)

T ^{0}C	**A**	**m**	**n**
20	237.587	5.832874	1
400	190	6.14	0.87
550	155	7.58	0.6
650	145	8.5	0.45

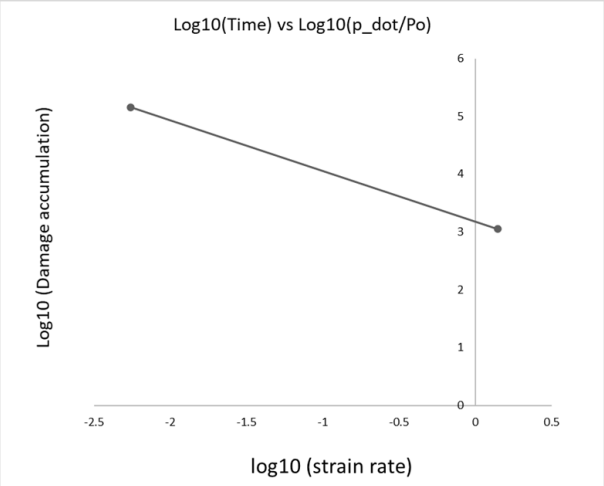

Figure 4.22. Log-log plot of strain rate vs damage accumulation to estimate parameters [17]

4.3.1 Fatigue Life Prediction and Correlation

In Ansys, the damage rate equation has been implemented using an ACT. After simulating the life at LCF, LCFC and TMF test it is observed that the calibrated values correlate well for LCF test (both at 0.003/s and 0.00001/s) and LCFC tests at 20°C, 400°C and 550°C. At 650°C the model correlates only at LCF at 0.003/s. Also, the TMF correlations are not satisfactory. Figure 4.23 shows experimental and simulated life correlation.

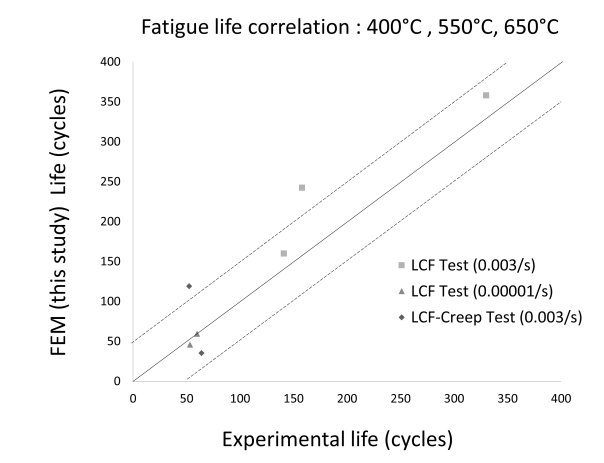

Figure 4.23. Experimental and Simulated Fatigue life correlation at LCF, LCFC test at 20°C , 400°C, 550°C and 650°C [21]

4.4 Unified Viscoplasticity Model Comparison Between Thesis and M. Bartosak

The chaboche Viscoplastic model has been modified by several researchers to simulate a unique mechanical behaviour of the material under study. The constitutive model is essentially based upon a flow rule and Chaboche -Nonlinear kinematic hardening rule, but each model consists of several added features to simulate a particular behaviour of the material.

Amongst them M.Bartosak [22] developed a Unified Viscoplastic material model and applied to simulate the response of SiMo4.06 under LCF and TMF loadings.Current research has also applied a unified viscoplastic model to simulate SiMo4.06 under isothermal LCF, LCFC and TMF loading conditions, but with a different formulations and features. Following section elaborates over the distinction between Unified Viscoplasticity model of M.Bartosak and Current research.

4.4.1 Objective

- **M.Bartosak:** The objective is Simulation of entire deformation history and its cyclic evolution throughout the LCF and TMF loading history (initial cycle to end of life cycle)
- **Thesis Research:** The objective is Simulation of only stabilised hysteresis loop in response to LCF, LCFC and TMF loadings

4.4.2 Features

M.Bartosak:

1. Combined Isotropic + Kinematic hardening
2. Strain-rate hardening dependency
3. Strain range dependency
4. Static recovery and dynamic recovery
5. Mean stress evolution

Thesis Research:

1. Only kinematic hardening model
2. Strain-rate hardening dependency
3. No strain-range dependency
4. Static + Dynamic recovery
5. No mean stress evolution

4.4.3 Formulations : Flow Rule

M.Bartosak

This model is based upon a Hyperbolic sine flow rule which gives a non-linear relationship between plastic strain rate and viscous stress as shown in the (x = back stress, k = initial yield stress, R=isotropic hardening/softening function) [3], [22]

$$\dot{p} = \frac{\partial \Omega}{\partial f} = \alpha \sinh\langle \beta f \rangle \tag{4.3}$$

Where, stress function is given by,

$$f(\sigma - x) = J(\sigma - x) - k - R \tag{4.4}$$

Thesis research

The flow rule in Thesis model is based upon a classical Norton law called as Perzyna viscoplastic model. This model shows nearly linear relationship between plastic strain rate and stress [3], and the constitutive equation is

$$\dot{\hat{\varepsilon}}_{pl} = \sum_{\mathrm{i}=1}^{n} \gamma_{\mathrm{i}} \left(\frac{\sigma}{\sigma_o} - 1 \right)^{1/m_{\mathrm{i}}} \tag{4.5}$$

4.4.4 Formulations : Hardening Rule

M.Bartosak

A combined Isotropic and kinematic hardening rule has been applied in this case. The isotropic hardening simulates the cyclic hardening/ softening. Whereas kinematic hardening allows a combination of multiple back stresses to improve the prediction of the hysteresis loop shape. The combined model is therefore enabling cyclic evolution of internal variables.

The stress function for the combined hardening involves the isotropic hardening function R along with back stress x [22], as shown below.

$$f(\sigma - x) = J(\sigma - x) - k - R \tag{4.6}$$

$$R = Q\left(1 - \mathrm{e}^{-k^p}\right) \tag{4.7}$$

Thesis Research

Only Non-linear kinematic hardening rule is incorporated here to predict the hysteresis loop behavior in response to cyclic loading. Since the damage rule for Thesis thesis was incremental in form, only stabilized loop is required to simulate, and so isotropic hardening was excluded.

The stress function involves only the back stress and initial yield stress (k) as shown below.

$$f(\sigma - x) = J(\sigma - x) - k \tag{4.8}$$

4.4.5 Formulations : Back Stress Terms

M.Bartosak

The back stress in the above equation is represented by the following equation:

$$\dot{\boldsymbol{x}}_{\mathrm{i}} = \frac{2}{3} C_{\mathrm{i}} \dot{\varepsilon}^{pl} - \gamma_{\mathrm{i}} \left(\boldsymbol{x}_{\mathrm{i}} - \boldsymbol{Y}_{\mathrm{i}}\right) \dot{p} - \gamma_r \left[J\left(\boldsymbol{x}_{\mathrm{i}}\right)\right]^{m-1} \boldsymbol{x}_{\mathrm{i}} \tag{4.9}$$

The second term in the above equation is the dynamic recovery term which introduces non-linearity in the evolution law. This term is modified further to include evolution of mean stress by adding a second order tensor Yi [22], which is given by following equation:

$$Y_{\mathrm{i}} = -\alpha_b \left(Y_{st} \frac{\boldsymbol{x}_{\mathrm{i}}}{J\left(\boldsymbol{x}_{\mathrm{i}}\right)} + \boldsymbol{Y}_{\mathrm{i}}\right) \left[J\left(\boldsymbol{x}_{\mathrm{i}}\right)\right]^m \tag{4.10}$$

Where ab and Yst controls the mean stress evolution.

Thesis research

The backstress in the above equation is given by following equation:

$$\dot{\boldsymbol{\alpha}}_{\mathrm{i}} = \frac{2}{3} C_{\mathrm{i}} \dot{\boldsymbol{\varepsilon}}^{pl} - \gamma_{\mathrm{i}} \hat{\varepsilon}^{pl} \boldsymbol{\alpha}_{\mathrm{i}} + \frac{1}{C_{\mathrm{i}}} \dot{C}_{\mathrm{i}} \boldsymbol{\alpha}_{\mathrm{i}} - \frac{C_{\mathrm{i}}}{M_{\mathrm{i}}^{m_{\mathrm{i}}}} \bar{a}_{\mathrm{i}}^{m-1} \boldsymbol{\alpha}_{\mathrm{i}} \tag{4.11}$$

Whereas there is no mean stress evolution considered here since cyclic evolution is not the scope of simulation.

4.4.6 FEA Implementation

M.Bartosak

This material model has been implemented in finite element software Abaqus. The model uses an implicit integration scheme also known as radial return method, and the author has developed a material subroutine in Abaqus software that contains integration of constitutive equations together with the Jacobian matrix.

Thesis research

The material model in Thesis model has been implemented in Ansys software. The viscoplastic model is based upon a combination of build-in material models available in Ansys material model library.

4.4.7 Results Comparison : Stress-Strain Hysteresis

M.Bartosak

From the figure below, the line passing close to the dots is simulation result. The figure represents peak stress amplitude evolution from first cycle to end of life. This M.Bartosak model simulated entire history of loading and cyclic evolution.

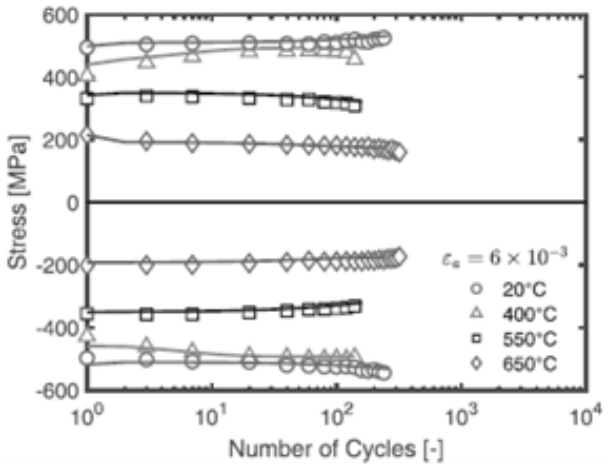

Figure 4.24. Cyclic stress evolution at strain amplitude = 0.006 a model corelation [22]

Thesis Research

This study is based upon an incremental damage rule as discussed in chapter-2, section 2.2. This defined the requirement of the viscoplastic rule to simulate only stabilized hysteresis loops at each temperature in response to LCF, LCFC and TMF conditions. Thus, cyclic evolution has not been considered.

The model correlation for the stabilized stress-strain hysteresis loop for all the load cases are mentioned in section 4.1.1

4.4.8 Results Comparison : Low Strain Rates

M.Bartosak

This model has been able to correlate the simulated hysteresis loop with experimental data at high temperature and low strain-rates (0.00001/s) due to several added features in the model, one such correlation is below:

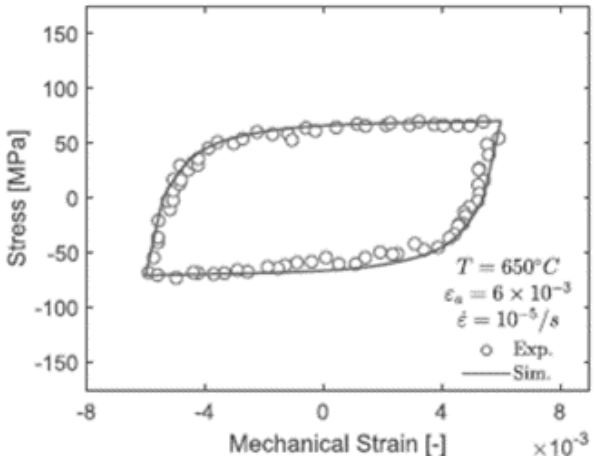

Figure 4.25. Hysteresis loop correlation at isothermal LCF at 650°C, strain amplitude = 0.006 [22]

Thesis Research

The prediction of hysteresis loop of this model has differences at peak temperature and low strain rate of 0.00001/s, as shown below.

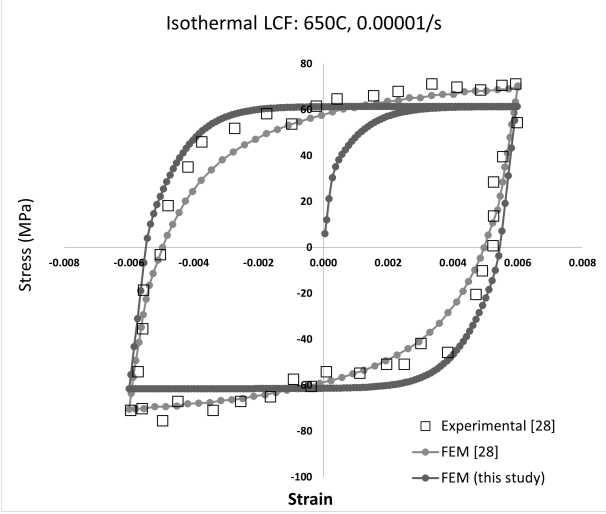

Figure 4.26. Stress-Strain Hysteresis comparison of Experimental [22], FEM [22], FEM (this study) at Isothermal 650°C LCF Test, 0.00001/s

4.4.9 Results Comparison : Stress Relaxation

M.Bartosak

The simulated stress relaxation at 400°C, 550°C and 650°C temperatures correlate well with experiments, one such correlation is shown in the figure below.

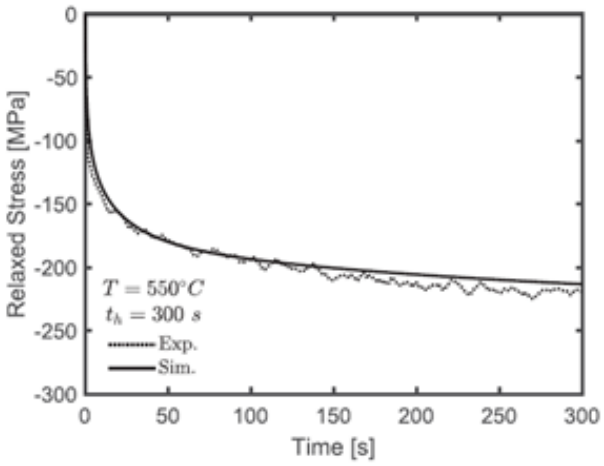

Figure 4.27. Simulated stress relaxation correlation at 550°C [22]

Thesis Research

Since both the models contains the static recovery terms, the simulated stress relaxation correlated well with the experimental results.

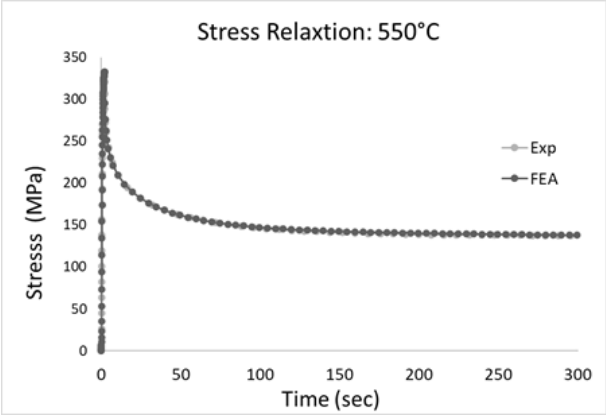

Figure 4.28. Experimental and FEA stress relaxation correlation at 550°C [22]

4.4.10 Results Assessment: Accuracy

M.Bartosak

The model has achieved good correlation with experimental isothermal LCF tests at strain rates ranging from 0.003/s to 0.00001/s under temperatures ranging between 20°C, 400°C and 550°C and TMF tests.

Thesis Research

The model correlation of stress strain hysteresis loops has been fairly good for isothermal LCF at 20°C, 400°C and 550°C for strain rates varying between 0.003/s to 0.00001/s, however the simulated results show differences at 650°C especially at lowest strain rate of 0.00001/s. A good correlation has been achieved in case of LCFC and TMF, as discussed in chapter 4.

4.4.11 Results assessment: FEA Implementation Ease

M.Bartosak

This model has been implemented using custom material subroutine which requires expert numerical integration and coding skills. It might not be feasible to develop a user subroutine for every FEA user. Since the constitutive equation is unique, the model parameter calibration and curve-fitting also need to be done by separately

Thesis Research

The thesis viscoplastic model has been implemented in Ansys software using a combination of material models using the Ansys build-in material model library. This method is easy to implement since the integration framework is provided by the software and it is easy to perform model calibration using build-in curve-fitting tool.

5. CONCLUSION AND FUTURE WORK

5.1 Conclusion

In this thesis, a methodology to implement unified viscoplasticity theory in FEM along with incremental lifetime damage model has been presented with major conclusions as follows:

1. A unified viscoplastic material model is implemented in FEA tool to model the deformations of Fe-3.2C-4.0Si-0.6Mo Cast Iron. The material model is capable of simulating material deformation dependency on temperature, strain-rates, hold time as is capable to modeling creep-stress relaxation and fatigue interaction

2. The material calibration techniques for calibrating the model parameters resulted to a fairly good correlation of FEA derived hysteresis loops with experimental hysteresis pertaining to Isothermal LCF (ranging from 0.00001/s to 0.003/s), Isothermal LCF-Creep tests (with hold time) and TMF responses. Thus, the viscoplastic model is successfully implemented and validated

3. An incremental damage rule has also been implemented in FEA. The FEA life predictions has been fairly good at room temperature (20C), 400C and 550C under Isothermal LCF (0.00001/s and 0.003/s) and LCF-Creep tests. The incremental damage model also predicted fatigue life at 650C only at LCF with 0.003/s test

5.2 Future Work

1. Improve calibration techniques for parameter estimation of damage model to predict Non-isothermal TMF life.

2. Improve the model capability to predict LCF and LCF-Creep life at higher temperatures and low strain rates

3. Apply the techniques for unified viscoplastic model and damage model development and calibration for other high temperature alloys

REFERENCES

[1] P. Andrade, *Thermo-mechanical fatigue, ansys white paper, ANSYS.INC*, 2020.

[2] J. Tong, Z.-L. Zhan, and B. Vermeulen, "Modelling of cyclic plasticity and viscoplasticity of a nickel-based alloy using chaboche constitutive equations," *International journal of Fatigue*, vol. 26, no. 8, pp. 829–837, 2004.

[3] R. Ahmed, P. R. Barrett, and T. Hassan, "Unified viscoplasticity modeling for isothermal low-cycle fatigue and fatigue-creep stress–strain responses of haynes 230," *International Journal of Solids and Structures*, vol. 88-89, pp. 131–145, 2016, ISSN: 0020-7683. DOI: https://doi.org/10.1016/j.ijsolstr.2016.03.012. [Online]. Available: https://www.sciencedirect.com/science/article/pii/S0020768316001311.

[4] K. Ikegami and Y. Niitsu, "Effect of creep prestrain on subsequent plastic deformation," *International journal of plasticity*, vol. 1, no. 4, pp. 331–345, 1985.

[5] D. Cojocaru and A. M. Karlsson, "A simple numerical method of cycle jumps for cyclically loaded structures," *International Journal of fatigue*, vol. 28, no. 12, pp. 1677–1689, 2006.

[6] P. von Hartrott, T. Seifert, and S. Dropps, "Tmf life prediction of high temperature components made of cast iron hisimo: Part i: Uniaxial tests and fatigue life model," *SAE International Journal of Materials and Manufacturing*, vol. 7, no. 2, pp. 439–445, 2014.

[7] J.-L. Chaboche, "Constitutive equations for cyclic plasticity and cyclic viscoplasticity," *International journal of plasticity*, vol. 5, no. 3, pp. 247–302, 1989.

[8] J.-L. Chaboche, "A review of some plasticity and viscoplasticity constitutive theories," *International journal of plasticity*, vol. 24, no. 10, pp. 1642–1693, 2008.

[9] W. Prager, "Recent developments in the mathematical theory of plasticity," *Journal of applied physics*, vol. 20, no. 3, pp. 235–241, 1949.

[10] C. O. Frederick and P. Armstrong, "A mathematical representation of the multiaxial bauschinger effect," *Materials at High Temperatures*, vol. 24, no. 1, pp. 1–26, 2007.

[11] N. Malinin and G. Khadjinsky, "Theory of creep with anisotropic hardening," *International Journal of Mechanical Sciences*, vol. 14, no. 4, pp. 235–246, 1972.

[12] *Academic research mechanical, release 2021 r1, help system, mechanical APDL theory reference, 4.4 rate independant plasticity ANSYS.INC*, 2021.

[13] Wikipedia contributors, *Recovery (metallurgy) - Wikipedia, the free encyclopedia*, (Accessed on 04/24/2021), 2020.

[14] I. Altair Engineering, *Efatigue - thermal mechanical technical background*, https://www.efatigue.com/hightemp/background/tmf.html, (Accessed on 04/24/2021), 2021.

[15] X. Xiao, H. Xu, J. Huang, J. Wang, and J. Zhang, "Stress relaxation properties and microscopic deformation structure in bending of the c7025 and c7035 alloy," *Crystals*, vol. 8, no. 8, p. 324, 2018.

[16] V. Kindrachuk, B. Fedelich, B. Rehmer, and F. Peter, "Computational methods for lifetime prediction of metallic components under high-temperature fatigue," *Metals*, vol. 9, no. 4, 2019, ISSN: 2075-4701.

[17] S. Majumdar and P. S. Maiya, "A Mechanistic Model for Time-Dependent Fatigue," *Journal of Engineering Materials and Technology*, vol. 102, no. 1, pp. 159–167, Jan. 1980, ISSN: 0094-4289. DOI: 10.1115/1.3224774.

[18] C. Sommitsch, R. Sievert, T. Wlanis, B. Günther, and V. Wieser, "Modelling of creep-fatigue in containers during aluminium and copper extrusion," *Computational Materials Science*, vol. 39, pp. 55–64, Mar. 2007. DOI: 10.1016/j.commatsci.2006.03.024.

[19] J. Schicker, D.-I. Sievert, B. Fedelich, D.-I. Klingelhöffer, and P.-D. Skrotzki, "Failure estimation of thermo-mechanically loaded hot parts in turbochargers," *MTZ worldwide*, vol. 71, Jun. 2010. DOI: 10.1007/BF03227025.

[20] M. Ekstrom, *Development of a ferritic ductile cast iron for improved life in exhaust applications — semantic scholar*, https://api.semanticscholar.org/CorpusID:137546664, (Accessed on 04/24/2021).

[21] X. Wu, G. Quan, R. Macneil, Z. Zhang, X. Liu, and C. Sloss, "Thermomechanical fatigue of ductile cast iron and its life prediction," *Metallurgical and Materials Transactions A*, vol. 46, no. 6, pp. 2530–2543, 2015. DOI: 10.1007/s11661-015-2873-9.

[22] M. Bartosak, M. Spaniel, and K. Doubrava, "Unified viscoplasticity modelling for a simo 4.06 cast iron under isothermal low-cycle fatigue-creep and thermo-mechanical fatigue loading conditions," *International Journal of Fatigue*, vol. 136, p. 105 566, 2020, ISSN: 0142-1123. DOI: https://doi.org/10.1016/j.ijfatigue.2020.105566. [Online]. Available: https://www.sciencedirect.com/science/article/pii/S0142112320300979.

[23] M. Bartosak, *Brief manual of scripts for thermo-mechanical fatigue predictions. prague, czech republic: Czech technical university in prague,faculty of mechanical engineering, department of mechanics, biomechanics and mechatronics, 2015.*

[24] J. KOSTAL, *Assessment of thermo-mechanical fatigue of exhaust manifold. brno, 2020. master's thesis. brno university of technology, faculty of mechanical engineering, institute of solid mechanics, mechatronics and biomechanics. 109 p.2020*, Available from: https://www.vutbr.cz/studenti/zav-prace/detail/121573, (Accessed on 04/24/2021).

[25] M. Bartosak, "Phenomenological models for lifetime prediction under low-cycle fatigue and thermo-mechanical fatigue loading conditions, a thesis submitted to the faculty of mechanical engineering, czech technical university in prague, in partial fulfilment of the requirements for the degree of doctor. prague, march," 2019.

[26] X. Wu, G. Quan, R. MacNeil, Z. Zhang, X. Liu, and C. Sloss, "Thermomechanical fatigue of ductile cast iron and its life prediction," *Metallurgical and Materials Transactions A*, vol. 46, pp. 2530–2543, 2015.

[27] N. E. Dowling, *Mechanical behavior of materials: engineering methods for deformation, fracture, and fatigue*. Pearson, 2012.

[28] ANSYS.Inc, *Academic research mechanical, release 2021 r1, help system, mechanical APDL theory reference, fitting parameters for a chaboche kinematic hardening model ANSYS.INC*, 2021.

PUBLICATIONS

Publications

- Lu, Z., Lyu, G., Gulhane, A., Park, H. M., Kim, J. S., Jung, Y. G., & Zhang, J. (2019). "Experimental and Modeling Studies of Bond Coat Species Effect on Microstructure Evolution in EB-PVD Thermal Barrier Coatings in Cyclic Thermal Environments." Coatings, 9(10), 626.

- Gulhane, A., Zhang, J., Yang, X., Lu, Z. et al., "Modeling of Temperature Swing Effect in Silica-Reinforced Porous Anodized Aluminum-Based Thermal Barrier Coating", SAE Int. J. Mater. Manf. 14(3):2021.

Presentations

- Gulhane, A., and Zhang, J. (2019). Computational modelling of thermal swing coatings and prediction of insulation performance. Oral Presentation at ASM Indianapolis Chapter Spring Conference, Columbus, IN

- Gulhane, A., and Zhang, J. (2019). Centrifugal Weeder. Poster presentation at Material Science and Technology Conference, Columbus, OH

- Gulhane, A., and Zhang, J. (2019). Computational Modeling of Thermophysical Properties of Silica Reinforced Porous Anodized Aluminum (SiRPA) Based Thermal Swing Coating. Poster and Oral presentation at International Conference on Powder Metallurgy And Particulate Materials (AMPM), Pheonix, AZ

Awards

- MPIF Student Grant Recipient, International Conference on Powder Metallurgy And Particulate Materials (AMPM), 2019, Pheonix, AZ